Vol.4 ,No.1, May 2017

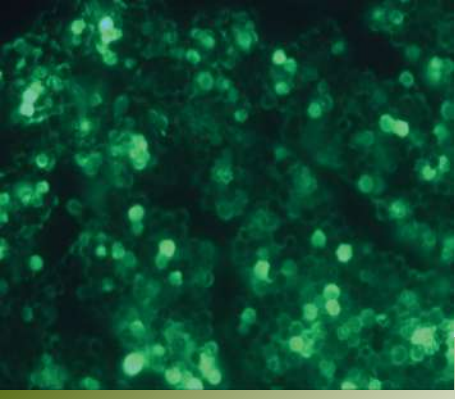

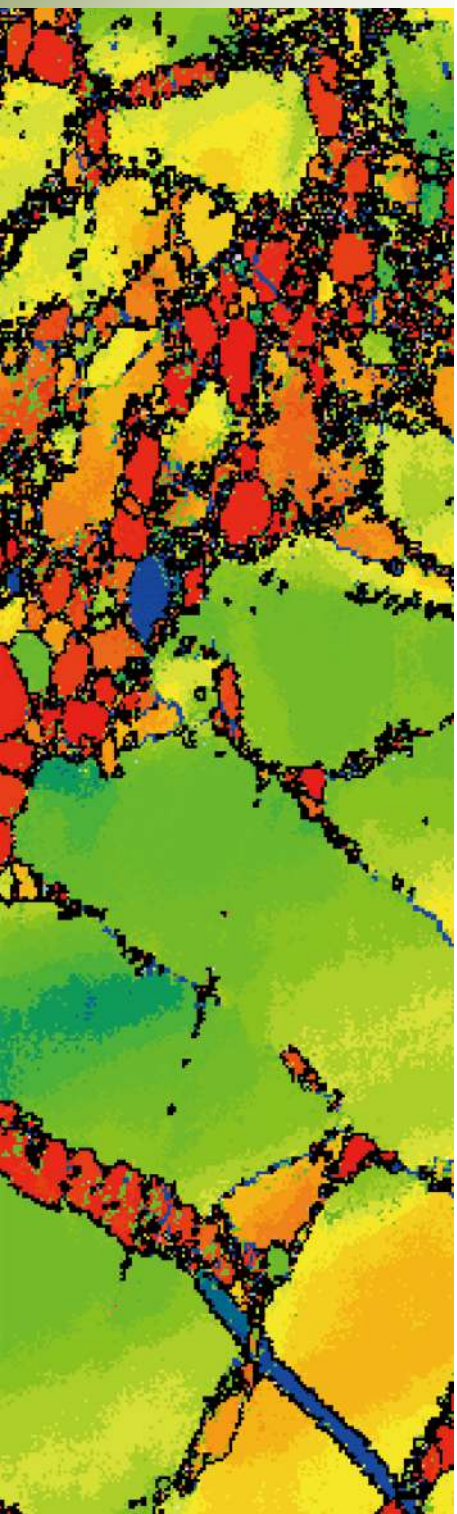

Transactions on GIGAKU

Special issue of The 5th International GIGAKU Conference in Nagaoka (IGCN), 2016

GIGAKU Press

Nagaoka University of Technology

Transactions on GIGAKU: Scope and Policy

Nagaoka University of Technology publishes an online, open access journal titled “Transactions on GIGAKU”, which is focused on the science and technology related to GIGAKU*. The mission of this journal is to spread out the concept of GIGAKU and the fruits of GIGAKU to the global world and to be a strong network for innovations in science and technology and for development of next generations of high-level human resources. This journal, therefore, covers research and education activities related to GIGAKU in broad areas.

* See ‘What is GIGAKU?’ below.

‘What is GIGAKU?’

GIGAKU is a term composed of two Japanese word-roots; GI and GAKU. The word GI〔技〕 literally stands for all kinds of arts and technology, and GAKU 〔学〕 stands for scientific disciplines in general when used as a suffix.

The term was originally coined to describe the fundamental philosophy of education and research of Nagaoka University of Technology (NUT) when it was established in 1976. Through this term the founders of NUT intended to express their recognition that all technical challenges in the real world require a scientific approach. And NUT has a relentlessly pursued GIGAKU since then.

Thirty-five years have passed and all surrounding conditions have changed dramatically during those years. We are witnessing rapidly globalizing economics and huge scale changes in demographic, industrial and employment structures. All those changes seem to necessitate the further evolution of GIGAKU. In response to this, NUT recently announced its new “Growth Plan” and a renewed definition of the term is given;

GIGAKU is a science of technologies, which gives us an angle to analyze and reinterpret diverse technical processes and objects and thus helps us to advance technologies forward. By employing a broad range of knowledge about science and engineering, management, safety, information technology and life sciences, GIGAKU provides us with workable solution and induces future innovations.

July 2012
Koichi Niihara, President of Nagaoka University of Technology

Submission and Publishing

"Transactions on GIGAKU" publishes original papers focusing on education, science, and technology related to GIGAKU. Proposals for special issues aligned with conferences are strongly encouraged*, and guest editors are welcomed. Papers submitted are peer-reviewed before publication. Publication charge is free for all submitted papers.

* Please contact to Editor-in chief, ywada@vos.nagaokaut.ac.jp

Copyright

Contact

joho-kiban@jcom.nagaokaut.ac.jp

(Revised May 2017)

Editorial board of special issue of The 5th International GIGAKU Conference in Nagaoka (IGCN), Vol.4, No.1. of Transactions on GIGAKU

Transactions on GIGAKU

Volume 4, No. 1, May 2017

The 5th International GIGAKU Conference in Nagaoka (IGCN)
(October 6-7, 2016, Nagaoka University of Technology, Nagaoka, Japan)

The IGCN is designed and organized to provide a cross-border, cross-sector, cross-disciplinary forum for those researchers, educators, and industrial leaders who are creating and practicing GIGAKU in various technology domains in various countries. Some papers presented in the IGCN are published in this first volume of Transactions on GIGAKU.

Table of contents

8. Pages 04008/1-6

Engineering Design Exercise (EDE) for Faculty Development in National Institute of Technology, Nagaoka College

Rumi Shindo Togashi , Taku Kiryu , Shigehiro Toyama , Yoshinori Tokoi , Tetsuro Iyama , Fujio Ikeda , Yuki Murakami , Shin-ichi Akazawa , Yasuko Tsuchida

Shape identification of cavity in structures using thermal testing data based on adjoint variable and finite element methods

Kotaro Maruoka[1,*], Takahiko Kurahashi[2], Tetsuro Iyama[3]**
[1)]Nagaoka University of Technology, 1603-1 Kamitomioka-cho, Nagaoka 940-2188, Japan,
[2)]Department of Mechanical Engineering, Nagaoka University of Technology, 1603-1 Kamitomioka-cho, Nagaoka 940-2188, Japan
[3)]Department of Mechanical Engineering, National Institute of Technology, Nagaoka college, 888 Nishikatakai, Nagaoka 940-8532, Japan

**E-mail: s133075@stn.nagaokaut.ac.jp*
***E-mail:kurahashi@mech.nagaokaut.ac.jp*

In this study, we introduced the smoothing techniques into the three-dimensional shape identification analysis of the cavity shape in test piece based on thermal data and compared diference between computational results employing each techniques. As a result, it is found that appropriate smoothing technique on the shape identification analysis varies according to conditions in target shape. Gaussian filter is appropriate in a case where the shape of cavity is identified as including smooother surface from the aspect of performance function. On the other hand, in the case that the cavity surface of the target shape has a dent, traction method has efficacy for bringing the computational model close to target shape.

1. Introduction

In the field of the shape optimization, there is the problem that the calculated sensitivities for the objective function become oscillation. Due to this problem, optimum shape is often obtained with concavo-convex surface. This problem is also seen in the shape identification analysis proposed by Kurahashi and Oshita[1], based on the adjoint variable method and the finite element method. In this analysis, identification of cavity shape is carried out by using temperature history on the thermal testing method. In previous study, Kurahashi et al. applied shape identification analysis to the cavity shape in test piece created using a 3D printer and introduced Gaussian filter, a kind of smoothing process, to modify the oscillation of the gradient vector[2]. As a result, identified shape close to target shape was obtained. However, appropriate condition for smoothing on the shape identification has not been investigated. In this study, we carry out shape identification analysis with two smoothing techniques, Gaussian filter and traction method[2]. The computational results are compared to characterize each processes on some computational conditions.

2. Shape identification analysis

The computation approach in shape identification analysis is shown in this section by reference to previous research[3]. State equation is given as heat transfer equation (See Eq. (1)).

$$\rho c\dot{\phi} - \kappa\phi_{,ii} = 0 \tag{1}$$

For the heat transfer equation, the initial condition and boundary condition are defined as in Eq. (2).

$$\begin{cases} \phi = \hat{\phi}(t_0) \quad \text{in} \quad \Omega \\ \phi = \hat{\phi} \quad \text{on} \quad \Gamma_1 \\ -\kappa\phi_{,i}n_{,i} = h_1(\phi - \phi_{inf}) \quad \text{on} \quad \Gamma_2 \\ -\kappa\phi_{,i}n_{,i} = h_2(\phi - \phi_{cav}) \quad \text{on} \quad \Gamma_3 \end{cases} \tag{2}$$

where ρ, c, κ, n_i , h_1, h_2, $\phi_{inf}$and ϕ_{cav} denote density, specific heat, thermal conductivity, unit normal vector, the convective heat transfer coefficient of the space inside the cavity, the convective heat transfer coefficient of the outside surface, ambient temperature and the temperature inside the cavity. Γ_1 denotes the lower surface, Γ_2 denotes the outside surfaces, and Γ_3 denotes the surface of the cavity (See Fig. 1).

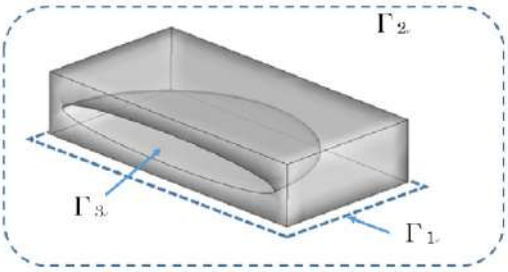

Fig. 1 Boundary definition of the test piece

The performance function is given as Eq. (3) to evaluate residual error between observational data and computational temperature

$$J = \frac{1}{2}\int_{t_0}^{t_f}\int_{\Omega} R(\phi - \phi_{obs})^2 d\Omega\, dt \tag{3}$$

From the state equation and the performance function, following Lagrangian function is obtained.

$$J^* = J + \int_{t_0}^{t_f}\int_{\Omega} \lambda(\rho c\dot{\phi} - \kappa\phi_{,ii}) d\Omega\, dt \tag{4}$$

This function indicates performance function added constrained conditions, i.e., the state equation, the boundary conditions and the initial condition. The first variation, which is a necessary condition for minimizing the Lagrangian function, is shown in Eq. (5).

$$\delta J^* = \frac{\partial J^*}{\partial \lambda}\delta\lambda + \frac{\partial J^*}{\partial \dot{\phi}}\delta\dot{\phi} + \frac{\partial J^*}{\partial \phi}\delta\phi + \frac{\partial J^*}{\partial x_i}\delta x_i \tag{5}$$

where x_i indicates coordinates on the design variable. The stationary condition is given as a condition under which each term equals zero. Then final term in Eq. (5) indicates the gradient vector with respect to the coordinates on the cavity surface. The cavity shape is updated with the gradient vector, and followed by recalculation of the state equation. The procedure for inverse analysis is described below.

(1) Set of initial coordinates $x_i^{(0)}$ and convergence criterion ε.
(2) Computation of state equation.
(3) Computation of performance function $J^{(0)}$.
(4) Computation of adjoint equation.
(5) Update of coordinate $x_i^{(l)}$ based on the computed gradient vector $\left\{\frac{\partial J^{*(l)}}{\partial x_i}\right\}$.
(l is the number of iterations, W is weighting parameter.)

$$\left\{x_i^{(l+1)}\right\} = \left\{x_i^{(l)}\right\} - [W^{(l)}]^{-1}\left\{\frac{\partial J^{*(l)}}{\partial x_i}\right\}$$

(6) Checking for convergence; if $(J^{(l)} - J^{(l+1)})/J^{(0)} < \varepsilon$, then stop, else go to step 7.
(7) Computation of state equation.
(8) Computation of performance function $J^{(l+1)}$

(9) Updating of weighting parameter $W^{(l)}$
I. if $J^{(l+1)} < J^{(l)}$, then $W^{(l)} = W^{(l)} \times 0.9$, and go to step 4
II. if $J^{(l+1)} > J^{(l)}$, then $W^{(l)} = W^{(l)} \times 2.0$, and go to step 5

3. Computational conditions

In previous study, thermal testing was carried out by using real test piece made of ABS. Fig. 2 shows detail of the test piece, and Fig. 3 shows finite element model. Considering the fact that it is easy to make the test piece by the 3D printer, the size and the shape of cavity is decided. The observation point is positioned on the center of the top surface. We describe the computational condition that the cavity shape shown in Fig.2 is set to target shape "Case A". Thermal conditions for the test piece and computational conditions are referred to previous study and given as shown in Tabs. 1 and 2. In addition, using another test piece incorporating the cavity with a dent, the heat transfer analysis is carried out, and the temperature at the observation point is obtained. The drawing of the model and finite element model are shown in Figs. 4 and 5. The computational condition setting target shape as the cavity shape shown in Fig.4 is described "Case B". In computation of shape identification, the initial shape model is given as incorporating a cavity thickness of 13 mm.

Table 1 Thermal properties of test piece

	Density ρ	Specific heat c	Thermal conductivity κ	Heat transfer coefficient	
				Outside surface	Cavity
	[g/cm^3]	[J/kgK]	[W/mK]	[W/m^{2}K]	[W/m^{2}K]
ABS	0.75	1386	0.1354	10.0	7.0

Table 2 Computational conditions

Total number of nodes	1460
Total number of elements	5552
Total time t_{max}, sec	600
Time increment Δt, sec	10
Time steps	60
Convergence criterion ε	10^{-6}

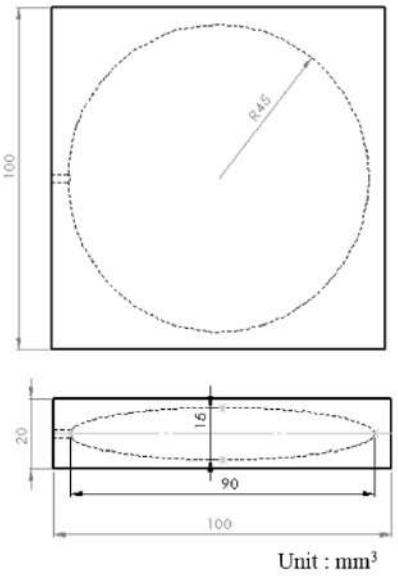

Fig. 2 Drawing of the test piece (1)

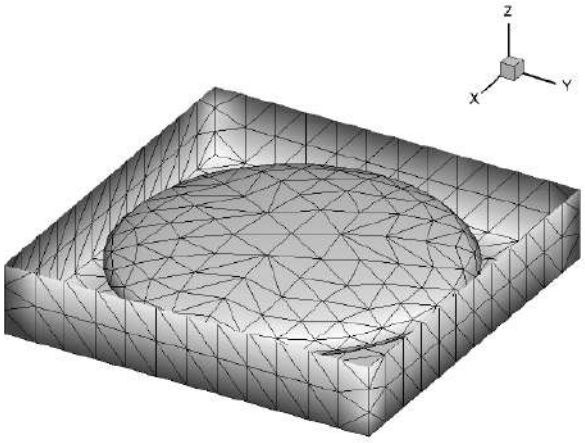

Fig. 3 Finite element model of the target shape (1)

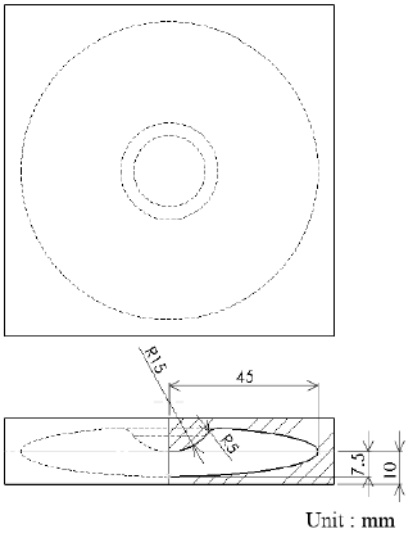

Fig. 4 Drawing of the test piece (2)

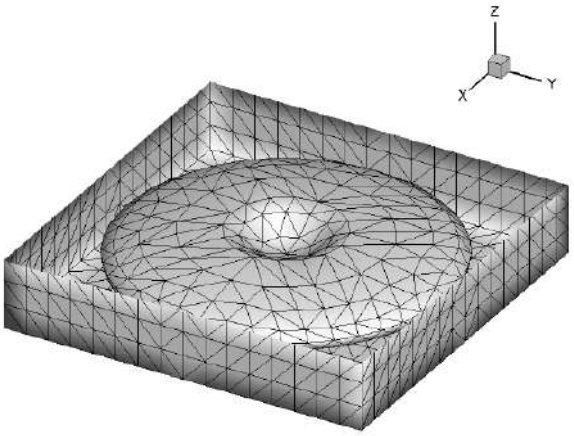

Fig. 5 Finite element model of the target shape (2)

4. Shape identification analysis introduced smoothing method

Shape identification analysis under the computational condition ”Case A” is carried out. First, numerical computation without the smoothing is carried out. The identified shape of the cavity is shown in Fig. 6. The cavity surface is identified convexly. In addition, normalized performance function decreases to about 0.55 (See Fig. 7). Thus the identified shape similar to target shape cannot be obtained. Next we applied Gaussian filter to gradient vector. Gaussian filter is one of the digital filter used in the field of graphics[4]. In this smoothing method, smoothed values are determined of all the nodes on target domain and weight parameter shown in Eq. (6)

$$G(x,y) = \frac{1}{2\pi\sigma^2} e^{-\frac{-x^2+y^2}{2\sigma^2}} \tag{6}$$

where x and y indicate the x-axial distance and the y-axial distance between the target node and referenced node. In this study, the weighting parameter for node m to node n is defined as Eq. (7)

$$G^{(m,n)} = \frac{\frac{1}{2\pi\sigma^2} e^{-\frac{(x^{(m)}-x^{(n)})^2+(y^{(m)})^2}{2\sigma^2}}}{\sum_{n=1}^{cx} \frac{1}{2\pi\sigma^2} e^{-\frac{(x^{(m)}-x^{(n)})^2+(y^{(m)})^2}{2\sigma^2}}} \tag{7}$$

where cx is the number of nodes on the surface, $x^{(m)}$ and $y^{(m)}$ denote the x-coordinate and the y-coordinate of node m. Then the shape identification introducing the Gaussian filter that parameter σ is set 20 is carried out. The identified shape of cavity is shown in Fig. 8. As a result, the shape of the cavity becomes smoother and performance function at final iteration decreases in comparison with the computational result without smoothing process (See Fig. 9). On the other hand, it is known that the traction method is a smoothing technique that the displacement filed is obtained as velocity field by using the gradient vector, elastic equation and boundary conditions[5]. Then elastic coefficient E and Poisson ratio v are given as 1 and 0, and gradient vector is smoothed from solution of the elastic deformation analysis that the computational model is assumed as elastic body. Computational results applying the traction method are shown below. Fig.10 shows the identified cavity shape. It can be seen that there is no big difference in comparison with the identified shape without smoothing. In addition, performance function at final iteration is more than the case without smoothing method (See Fig. 11).

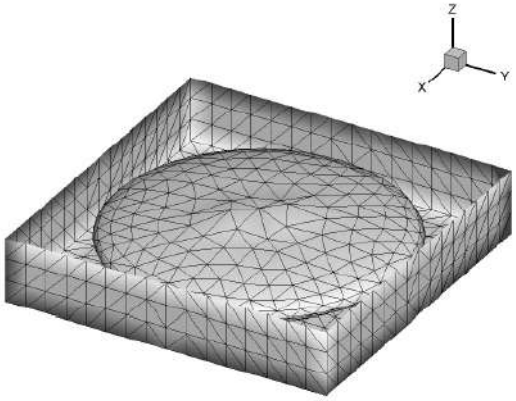

Fig. 6 Identified cavity without smoothing in Case A

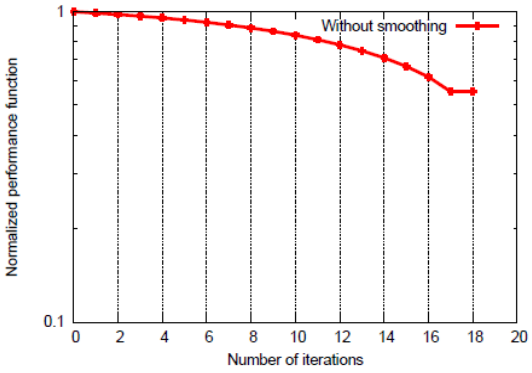

Fig. 7 Variation of normalized performance function without smoothing in Case A

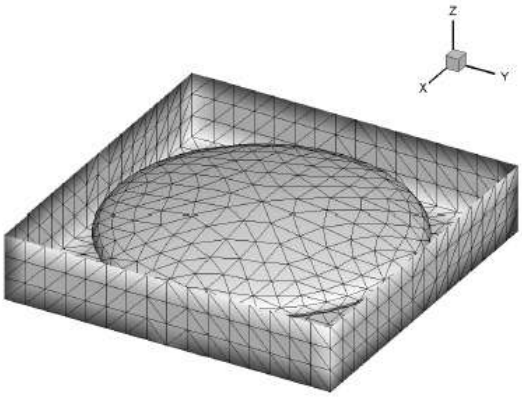

Fig. 8 Identified cavity with Gaussian filter in Case A

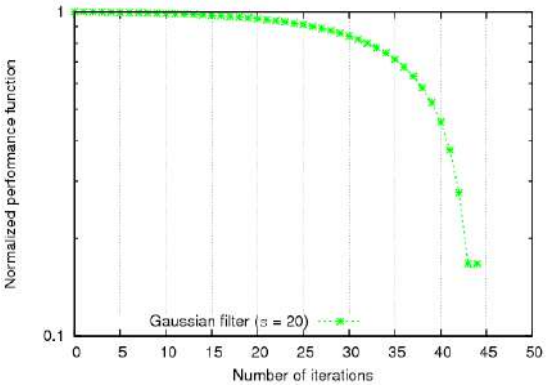

Fig. 9 Variation of normalized performance function with Gaussian filter in Case A

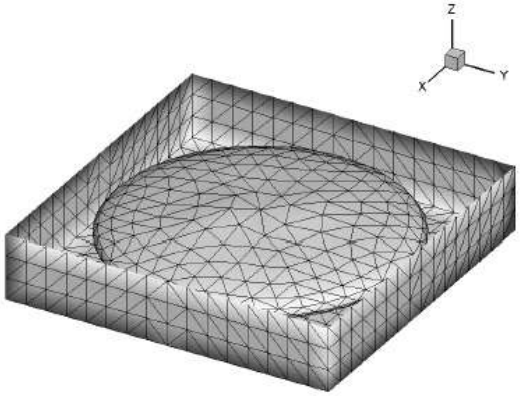

Fig. 10 Identified cavity with traction method in Case A

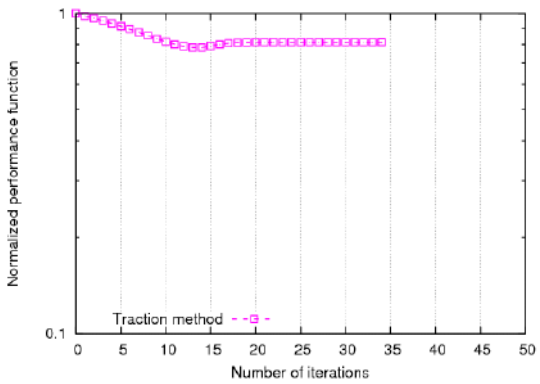

Fig. 11 Variation of normalized performance function with traction method in Case A

Moreover, shape identification analysis applying computational condition “Case B” are also carried out. Figs.12 and 13 show the computational results without smoothing method. As a result, undulation of the inner surface can be seen in the identified cavity. Figs.14 and 15 show the cavity shape at final iteration in computation applying the Gaussian filter and the variation of the normalized performance function, respectively. It can be seen that the surface of the cavity has a dimple similar to target shape. On the other hand, identification accuracy is not higher than the case

without smoothing method by performance function. And computational results using the traction method are shown in Figs. 16 and 17. It is seen that the identified cavity surface is more concavo-convex than the result applying Gaussian filter (See Fig. 16). In addition, the value of the performance function at final iteration decreases in comparison with the result without smoothing.

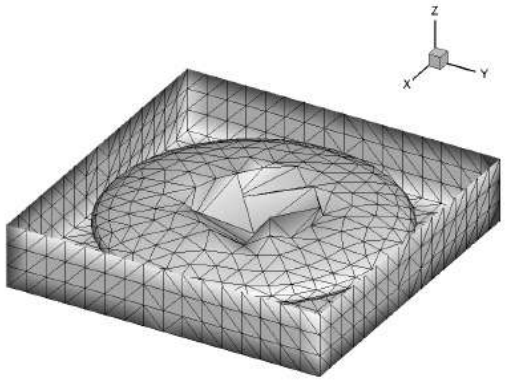

Fig. 12 Identified cavity without smoothing in Case B

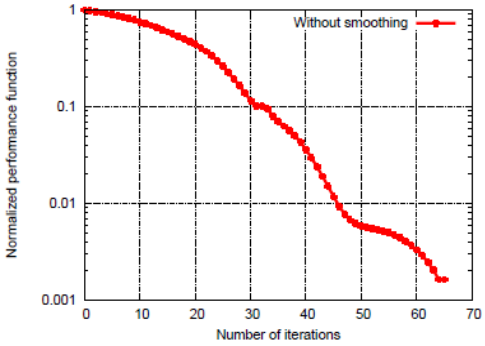

Fig. 13 Variation of normalized performance function without smoothing in Case B

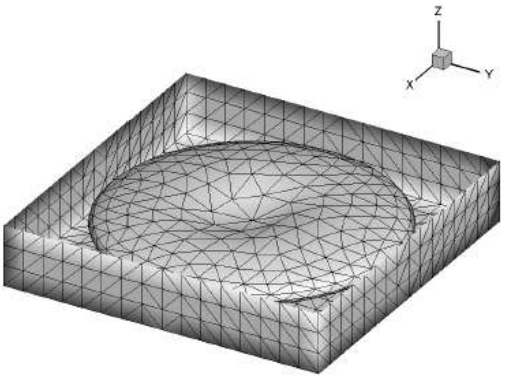

Fig. 14 Identified cavity with Gaussian filter in Case B

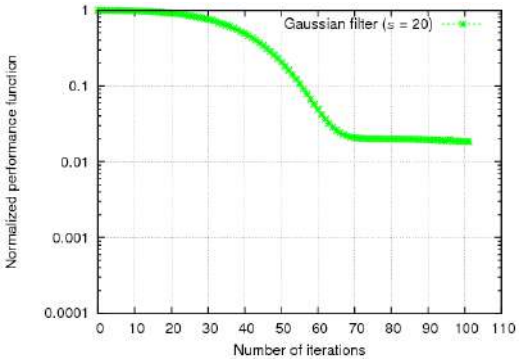

Fig. 15 Variation of normalized performance function with Gaussian filter in Case B

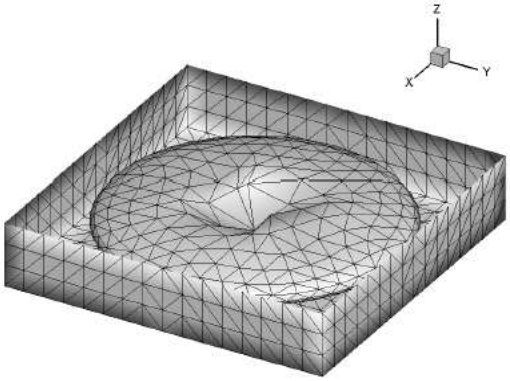

Fig. 16 Identified cavity with traction method in Case B

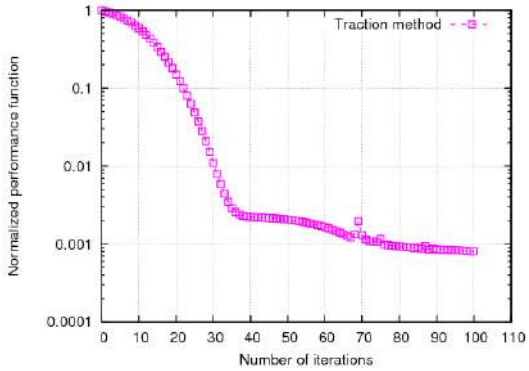

Fig. 17 Variation of normalized performance function with traction method in Case B

Finally, variations of normalized performance function for each conditions are shown in Figs. 18 and 19. In addition, Figs 20 and 21 show the comparison of the temperature at the observation point

in each condition. In these figures, the temperature in each case is result at the final iteration. In Case A, performance function at final iteration in iterative computation with the Gaussian filter is smallest value. On the other hand, it is found that the performance function at final iteration can be minimized by applying traction method in Case B. Similarly, in Figs 20 and 21, it is seen that temperature at final iteration with the Gaussian filter is the closest to the observed temperature in all cases in Case A, and the temperature at final iteration with the traction method is the closest to the observed temperature in all cases in Case B. Therefore, it can be said that the suitability of the application of each smoothing method depends on the shape of the cavity. Moreover, it appears that if the appropriate smoothing method is employed in the cavity shape identification, the value of performance function minimize, i.e., the temperature at the target point is close to the observed temperature, in comparison with that without smoothing method.

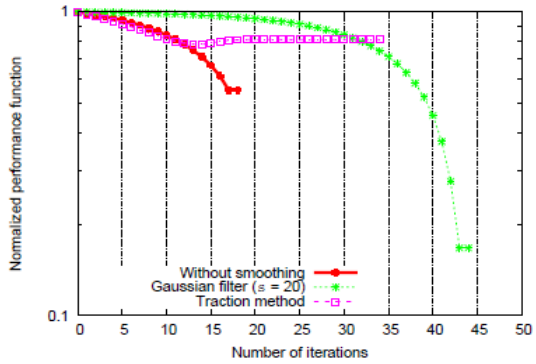

Fig. 18 Comparison of normalized performance function in Case A

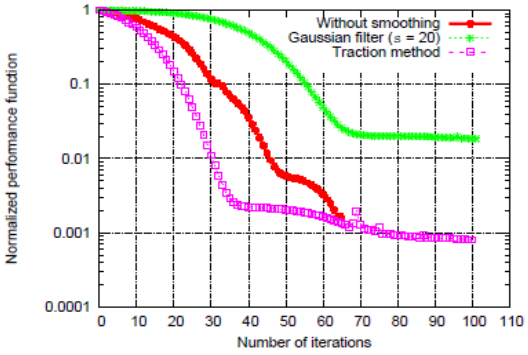

Fig. 19 Comparison of normalized performance function in Case B

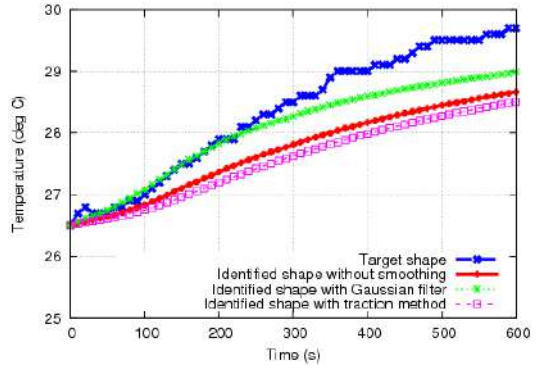

Fig. 20 Time history of the temperature on the identified shape in Case A

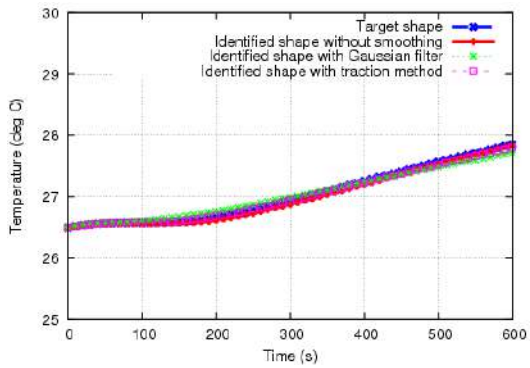

Fig. 21 Time history of the temperature on the identified shape in Case B

5. Conclusions

In this study, the comparison of the smoothing technique employed in three-dimensional shape identification analysis for cavity in the resin structure was carried out. As for computational condition, target shape was given as two type of model, and the Gaussian filter and the traction method were employed as smoothing method. Results in this study are shown below.

(1) The Gaussian filter is effective for minimization of performance function in case of the target shape with smoother surface.
(2) If the target shape is given as including a cavity with convex surface, the result applying the traction method is better than that applying the Gaussian filter.

Acknowledgments

This work was supported by the Program for High Reliable Material Design and Manufacturingat Nagaoka University of Technology and a 2015 Grant for Joint Research between Nagaoka College and Nagaoka University of Technology. The computations were mainly carried out using the Fujitsu PRIMERGY CX400 computer facilities at Kyushu University's Research Institute for Information Technology.

References

[1] T. Kurahashi and H. Oshita, Problem of Partial Reinforcement Corrosion in Concrete Using Observed Temperature on Surface, Journal of The Japan Society for Industrial and Applied Mathematics, **21, 3** (2011) 221-240.

[2] H. Azegami and Z. C. Domain, Optimization Analysis in Linear Elastic Problems (Approach Using Traction Method), Journal of The Japan Society of Mechanical Engineers, **60, 578** (1994) 144-150.

[3] T. Kurahashi, K. Maruoka and T. Iyama, Numerical shape identification of cavity in three dimensions based on thermal non-destructive testing data, Engineering Optimization, **1-17** (2016).

[4] H. Okuda and K. Deguchi, Gray Level Edge Behavior for the Gaussian Blurring Filters and Its Application to Edge Extractions, Journal of Information Processing Society of Japan, **10, 36** (1995) 2244-2251.

[5] D. Fujii and J. Kakita, Shape optimization of frame structures using traction method, Journal of Structural and Construction Engineering, **682, 77** (2012) 1881-1886.

(Received: 5 September 2016, Accepted: 4 April 2017)

Optimizing boundary surface of ceramics die in deep drawing process

Hanh C. Nguyen[1], Shigeru Nagasawa[1,*], Kensei Kaneko[2]

[1)]Nagaoka University of Technology, Nagaoka, Japan 940-2188
[2)]National Institute of Technology, Nagaoka College, Nagaoka, Japan 940-8532
**E-mail: n_hanh@stn.nagaokaut.ac.jp*

The objective of the present study was to propose a new approach to optimize the geometry parameters of ceramics die in deep drawing process. The optimization problem has been formulated with the objective of optimizing the maximum principal stress in the full stroke of deep drawing process. In this study, FEM software was used to simulate the stress distribution on the die surface and predict the brittle cracking occurrence on the die surface. Accordingly, the optimum ellipsoid curvature on the curved surface of die hole can be obtained, and thus process design optimized.

1. Introduction

Due to its versatility, good strength and light weight design, deep drawing process is widely used in various applications, especially in automotive and aerospace industries. However, after a time working, a variation of surface roughness, wear, and surface cracks gradually appear on the die surface relating to many factors: die radius, punch radius, friction between the die and the worksheet, and so on.

In a forming process of U-cup drawing, for an example as shown in Fig.1, a ceramics (Si_3N_4) die was recently tried to be used for pressing a 2mm thickness mild carbon steel disk, the diameter of which has 36mm, by using a 24.83mm diameter high carbon steel punch. In this case, due to a surplus high pressure on the entrance surface of die, a fracture occurred at the die body after several times repetitions. Figure 2 showed an example of cracked zone on the die surface. Observing the die surface with digital scanning microscope, we can detect many cracking positions at the arc-end of ceramics die with $L_{srf\text{-}dm}$ varying from 8mm to 9mm as was shown in the Fig.5. According to the stress analysis of worksheet without cracking on the die body, the Mises stress of worksheet and the principal stress of die block were numerically simulated and the stress states of them were relatively estimated. However, they can not predict the real fracture behavior neither its safety designing condition.

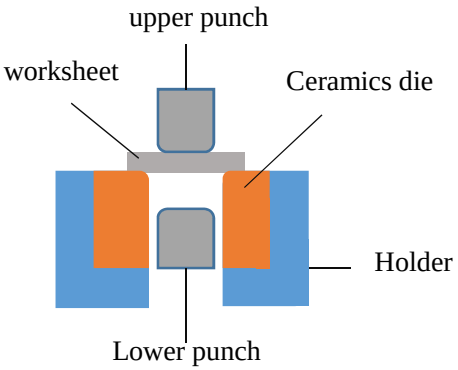

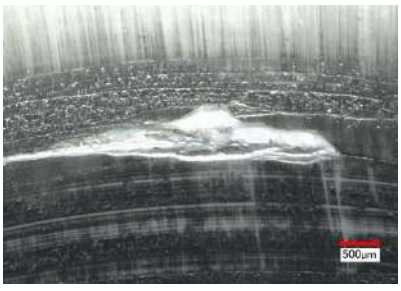

Fig. 1 Deep drawing process model for making U-cup **Fig. 2** A crack area on the ceramics die surface

Therefore, in this work, we propose a possibility and a methodology of prediction of cracking positon and how to evaluate the modification of tool design. In order to develop a prototype FEM model composed of elastic ceramic die body and a mild carbon steel in the axial symmetric condition, and also to predict the peak position trajectory of the maximum principal stress and maximum shear stress, a case study of the real production of U-cup shaped SPCE disk plate has been analyzed. This simulation model proposes an analysis

method for detecting the most severe point on a die surface, under specifying the radius of die hole and the critical strength of the dies body. At the result, some optimization parameters can be found for designing the boundary surface of the ceramics dies.

2. Finite element simulation setup

The deformation behavior of cylindrical deep drawing process is simulated by using MSC. Marc version 2015 system - the Finite Element Method (FEM) software. This simulation model consisted of an elasto-plastic body as a 2mm thickness worksheet of SPCE (mild carbon steel) and an elastic body as a ceramics die block. The mechanical properties of SPCE worksheet was shown in Table 1. The in-plane mechanical properties of the SPCE worksheet were experimentally evaluated by the uni-axial tensile testing based on the JIS-K7127. Figure 3 shows the relationship between the stress and strain under the tensile testing. The die body of ceramics (Si_3N_4) was assumed to have a little plastic deformation at the breaking strength of 360MPa which was gotten from the referenced tensile strength [1]. Generally, although the ceramics body such as Si_3N_4 appears to be an elastic-brittle material, when a sort of damage criteria is diagnosed in the tool body, a certain plastic yielding is virtually necessary for evaluating the damage level of the tool body. Therefore, a small breaking strain of ε_B= 0.0015 was virtually assumed here. This is used for detecting a severe-stressed point from the aspect of damage function such as Oyane's formula, Ayada's formula [2].

Table 1 Mechanical properties

	Material	Young's modulus GPa	Poison's ratio	Yield stress MPa
Worksheet	Carbon steel	205	0.3	190
Die	Si3N4	290	0.28	

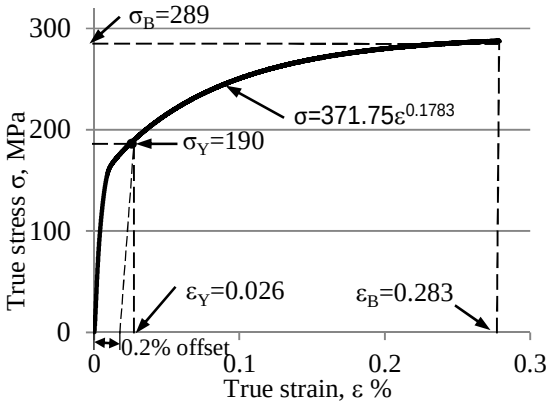

Fig. 3 Stress-strain curve of SPCE worksheet

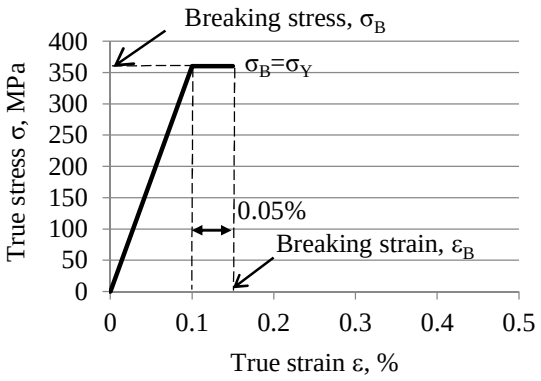

Fig. 4 Breaking behavior of Si_3N_4

Figure 5 shows schematics of initial worksheet stacked on the upper level of die and the geometrical relationship between the tool and the worksheet. Initially, the outside of working disk is attached to the entry round surface of die and the upper punch is indented to the top side of working disk until the punch moves to the stroke of 15.5mm. After releasing the upper punch from this pressing, the lower punch moves upward with the same velocity as that of upper punch elevation.

Figure 6 shows the velocity diagram of upper and lower punches. An FEM simulation of the U-cup drawing process was achieved in two stages. In the first stage, the upper punch moves down and acts upon the carbon steel disk with a punching force. In the second stage, the upper punch was released, and the lower punch moved up and acted upon the material with a punching force. In these two steps, both the upper punch and the lower punch moved at a quasi-static state. The time-dependent thermal effect was not considered here. For the sake of convenient execution, a virtual velocity of 2.5mm/s was assumed in MARC.

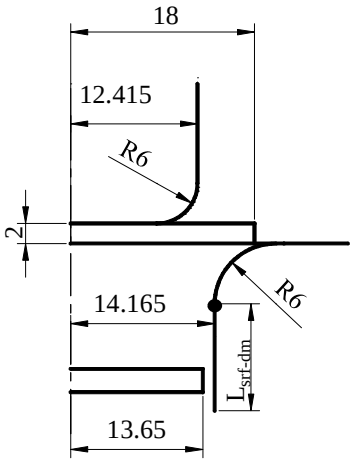

Fig. 5 Schematics of worksheet geometries (unit: mm) and cracking positions in the experiment

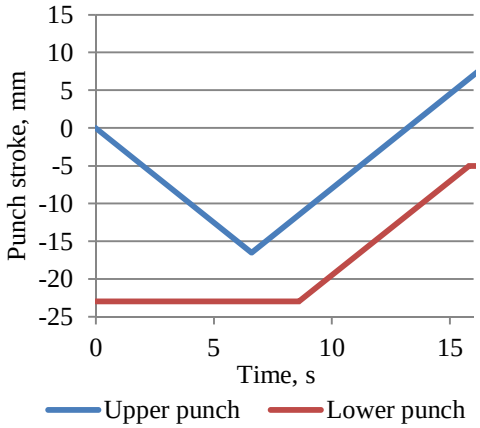

Fig. 6 Punch motion diagram

3. Stress distribution on the ceramics surface

Figure 7 shows the variation of the peak maximum value of maximum1st principal stress σp1 (MPa) and its occurred position Lsrf-p1 (mm) with respect to the upper punch displacement, while Fig.8 shows the variation of the maximum shear stress τ (MPa) and its occurred position Lsrf-ps (mm) with respect to the upper punch displacement. In this result, it is found that the peak of maximum shear stress occurred at the arc-end inside position of round surface: Lsrf-ps = 8.82mm (on the un-loading process), and also the peak of first principal stress occurred at the arc-end of round surface: Lsrf-p1= 10mm (on the loading process).

As a result, we can detect the critical point on the die body. It is useful for detecting the position of crack initiation on the ceramics die surface. Comparing this result with the experimental cracked position (Fig.5), we found that the cracked position was almost same as that of the peak maximum shear stress of τ. The position of σp1 was a little different position. Based on the FEM simulation, this work presented an analyzing method for determining the peaks of the maximum principal stress distribution as well as the maximum shear stress distribution on the die surface.

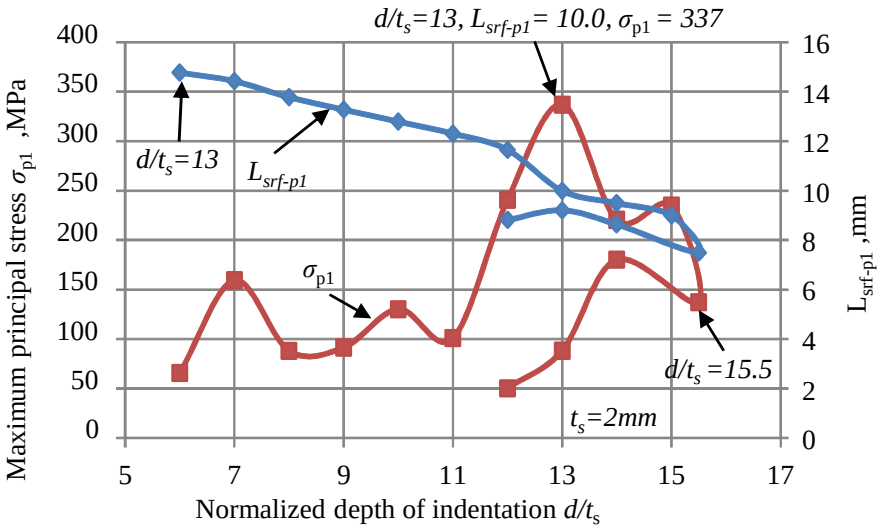

Fig. 7 Peak of maximum 1st principal stress

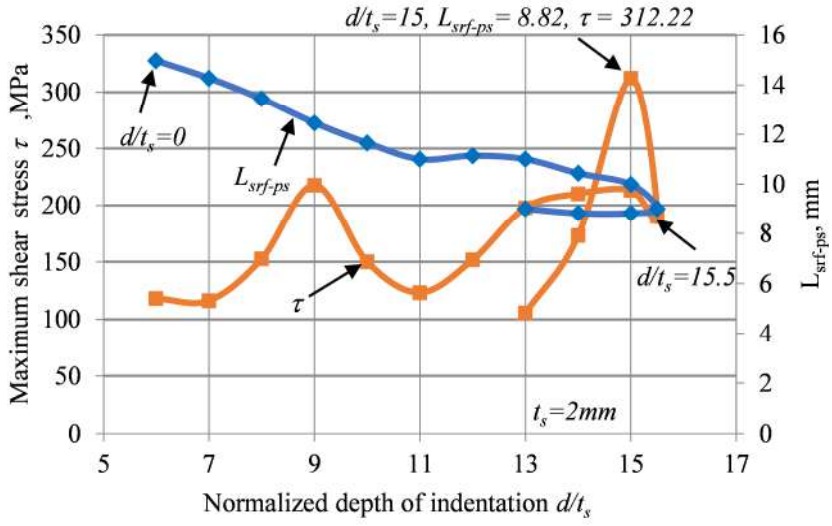

Fig. 8 Peak of the maximum shear stress

Prediction of severe position using a Damage model

Seeing the experimental result (Fig.2), cracks appeared on the die surface which could be because of many factors: die radius, punch radius, lubrication and so on. We used a method of predicting damage of drawing die which is assumed to be applicable for ductile fracture. In this work, the Cockroft-Latham Damage Indicator was considered in MARC [2] . It is often used in linear elastic fracture mechanics to predict brittle fracture [3, 4]. The objective of this work is to provide a method for predicting the damage of drawing die enabling to design of improved die surface by predicting brittle fracture under various conditions, and enabling us to design improved die surfaces. Fracture occurs when the damage factor has reached its critical value of C. Here, we assumed that C=0.32 in the model.

$$\int \frac{\sigma_{max}}{\bar{\sigma}} \dot{\bar{\varepsilon}} dt > C \qquad (1)$$

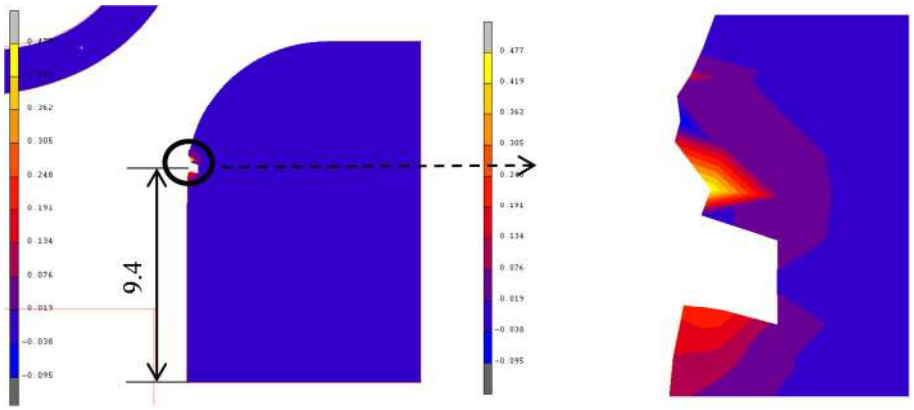

Fig. 9 Damage occurs at the arc-end position of round surface

In the case of assuming ε_B=0.15% for die body breaking strain, the crack occurred at the arc-end inside position of round surface: $L_{srf\text{-}dm}$=9.4mm, d/t_s=14.4., (on the un-loading process). The crack initiation characteristics obtained via simulation are close to those got through the physical experiment as was shown in Fig.5. The cracking position predicted by the simulation was shown in the Fig.9. This damage indicator is based on the effect of Maximum principal stress over the plastic strain path. Therefore, when we define ε_B=0.1% of breaking strain (perfect elastic linear behavior), this damage indicator can not detect the crack point on the die surface. However, this damage model is applicable to predicting the damage for another fragile material such as GFRP laminated sheet and the acrylic sheet.

4. Parameter analysis of entry radius of die surface

Many factors affect the sheet metal forming process such as die radius, friction coefficient, blank holder force, and so on. Optimizing these parameters is an important task to reduce product cost. The die radius has the greatest influence on the deformation behaviour of the deep drawing process (with an 89.2% influence), followed by friction force with a 6.3% influence and the blank holder force with a 4.5% [5]. To reduce the stress concentration on the die surface, we use appropriate ellipsoid curvature on the curved surface of die hole.

In this work, the authors presents a new approach to optimize the geometry parameters of die hole. The optimization problem has been formulated with the objective of optimizing the maximum principal stress in the full stroke of deep drawing process. The current die surface (Fig.10 (a)) is provided an ellipsoid curvature with r_d set at 6mm, and R_d varying between 5mm and 8mm. The geometry is created in SolidWorks – a CAD/CAM software [6] and imported to the MARC system as showed in the Fig.10 (b).

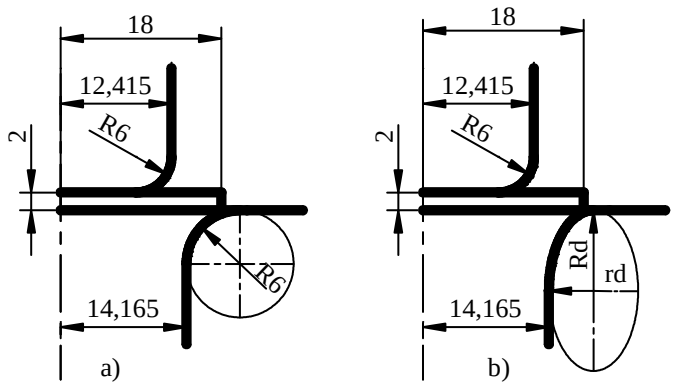

a. the current die surface b. variable ellipsoid curvature

Fig.10 Using appropriately curved surface of die hole

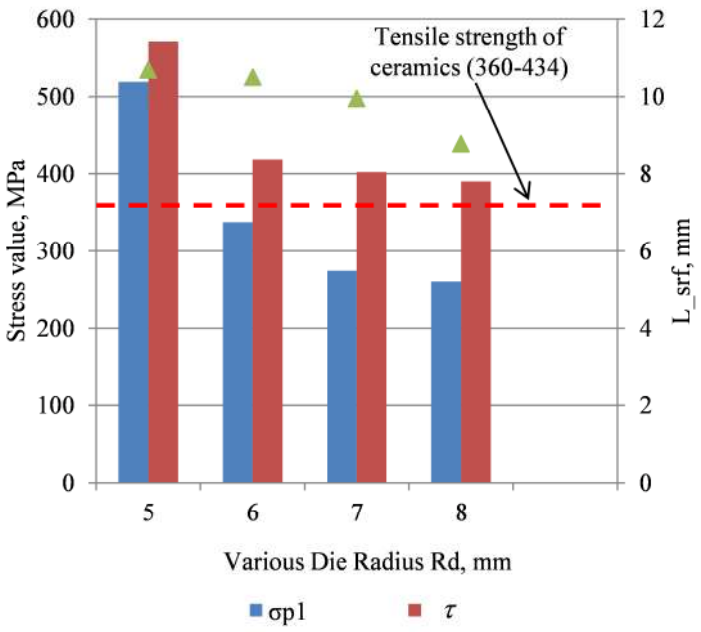

Fig. 11 Maximum principal stress and maximum shear stress in various die radius

To investigate the effect of entry radius on the stress distribution of die surface, different simulations with different die radius were performed. Whereas the material properties, the punch profile, and the clearance parameters are kept at the same conditions. The critical point occurs at the arc end of the die surface when the die radius is varied from 5 mm to 8 mm. From Fig.11, it is found that maximum principal stress and maximum shear stress of the drawn cups is decreasing as the die radius is increasing. However, when the die radius is increased, wrinkle formation will occur in the worksheet [7]. Therefore, 6 mm in R_d is recommended as an optimum value for this die fillet radius.

Punch force

Figure 12 shows the effect of the variation in die radius on punch force during the forming process, when the friction coefficent between worksheet and ceramics die is considered as Coulomb friction law with μ=0.23. When we increase the die radius, punch force tends to decrease. After the worksheet passes through the arc end of the die, the punch force suddenly increases because of the larger contact between the die surface and the worksheet.

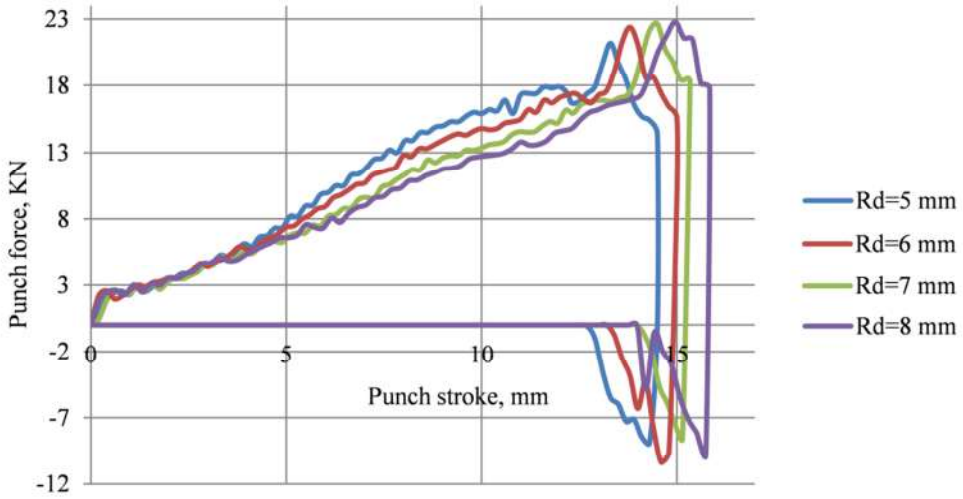

Fig. 12 Punch force required in various die radius

5. Conclusion

(i) In order to diagnose the strength state of die body, the authors proposed to watch a state point of the peak maximum principal stress and peak position (σp1, Lsrf-p1) in the die body for the full stroke motion. Plotting this state point (σp1, Lsrf-p1) with respect to the punch stroke, the most severe position and stress value were easily detected. It is found that this monitoring method is also useful for detecting an optimum design parameters.

(ii) Comparing the simulated stress severe position and the experimental failure position, they were well matched. This results verified a validity of developed simulation model for discussing the strength of die body made by ceramics.

(iii) This study also proposes a method of predicting brittle damage for ceramics die in deep drawing process and thus contributes to the design and parametric optimization of the ceramic dies.

Acknowledgments

This work was supported by a fund for developing a core of excellence as innovation and branding project, from the GIGAKU Innovation Promotion Center, NUT, 2014-2015. The authors thank for providing a case of prototype ceramics die from Shimizu Industrial Co.Ltd.

Nomenclature

Symbol	Definition
σ_{p1} or σ_{max}	Maximum principal stress, MPa
τ	Maximum shear stress, MPa
$L_{srf\ (p1,ps,dm)}$	Arc length (with 1st principal, shear maximum, damage), mm
d/t_s	Normalized depth of indentation, mm
$\bar{\sigma}$	Effective von Mises stress, MPa
$\dot{\bar{\varepsilon}}$	Effective elastic-plastic strain rate
C,	Material threshold for damage
R	Radius of circle of entry hole in die
R_d, r_d	Radius of elipsoid, in the long axis and short axis

References

[1] Ferro-Ceramic Grinding, I., Wakefield, Mass., "Material Properties Charts," https://www.ceramicindustry.com/ext/resources/pdfs/2013-CCD-Material-Charts.pdf.
[2] MSC Software, Marc® 2010 Volume A: Theory and User Information.
[3] Bouchard P.O., B. F., Chenot J.L., "Modeling of sheet metal cutting by coupling damage and crack propagation theories," Proc. simulation of Material processing: Theory, Methods and Applications, pp. 1001-1006.
[4] Goijaerts A. M., G. L. E., Baaijens F. P. T., 1999, "Prediction of Ductile Fracture in Metal Blanking," Journal of Manufacturing Science and Engineering, 122(3), pp. 476-483.
[5] Padmanabhan, R., Oliveira, M. C., Alves, J. L., and Menezes, L. F., 2007, "Influence of process parameters on the deep drawing of stainless steel," Finite Elements in Analysis and Design, 43(14), pp. 1062-1067.
[6] MSC Software, Release Overview - Marc 2014.
[7] Kakandikar G.M., N. V. M., 2007, "Optimization of Forming Load and Variables in Deep Drawing Process for Automotive Cup Using Genetic Algorithm," On-line Journal, http://www.optimization-online.org/DB_HTML/2007/03/1606.html.

(Received: 7 October 2016, Accepted: 6 April 2017)

Bending behaviour of polypropylene sheet subjected to two-line wedge indentation

Akihiro Yamamoto[1*], Satawat Singprayoon[2], Shigeru Nagasawa[1], Seksan Chaijit[3]
[1)] *Dept. of Mechanical Engineering, Nagaoka University of Technology, Nagaoka, Japan*
[2)] *Exchange research student in NUT from Pathumwan Institute of Technology, Bangkok, Thailand*
[3)] *Dept. of Mechatronics Engineering, Pathumwan Institute of Technology, Bangkok, Thailand*
**E-mail: akiyamamech@gmail.com*

In this paper, the bending characteristics of a 0.3mm thickness Polypropylene (PP) sheet subjected to a sharp two-line wedge indentation were investigated. Through the experiments, the formability of the scored zone was characterized with the groove depth and folding (normal and reverse wise) direction, and compared with that of Polyethylene Terephthalate (PET).

1. Introduction

Half-cutting of worksheets is a well known process and used for producing packaging boxes, especially for folding thick resin sheets [1,2,3]. The relationship between the mechanical conditions for the half-cutting and the folding profile of the worksheet are important characteristics to create a successful crease in a packaging box. The process of wedge indentation of a worksheet has been formally explained by Hesse [4] and Mizuguchi et al. [5] in their respective works on technology for packaging sheets. The most important mechanical conditions regarding the half-cutting are the cutting wedge profile, the indentation depth of the wedge and the material properties of the worksheet. On the other hand, the folding characteristics of wedged (scored) worksheet are mainly influenced by the deformation profile of the scored zone. This folding characteristics can be verified by studying the bending moment response regarding a certain folding angle. Empirically, the residual thickness after scoring (thickness of the worksheet minus the indentation depth of the wedge cutter) of the resin sheet is important in determining the quality of folded profile and keeping a certain strength on the hinge left after folding [3]. However, these folding characteristics seem be sensitive and change with respect to the material properties. Thus, there is a need to experimentally reveal the bending behavior of a worksheet with respect to the wedge indentation depth and the folding direction (normal and reverse wise).

Nagasawa et al. [6,7] have reported about the effects of scored residual thickness on the bending characteristics of a 0.5mm thickness Polyethylene Terephthalate (PET) board subjected to a two-line wedge indentation. Here, a laminated structure of three layers (G-PET/A-PET/G-PET) was investigated and the strength of laminated interface was discussed with respect to the scored residual thickness. The gradient of bending moment resistance for folding and the in-plane tensile strength of the grooved zone were also discussed for the specified PET sheet. However, this approach was not used to investigate other resin sheets.

Recently, thick sheets of Polypropylene (PP) are becoming more popular for producing transparent carton boxes. Although there are reports of usage and fundamental properties [1,8], and re-

search articles have been reported for cutting strength [9,10], there are not almost any academic reports regarding the half-cut folding of PP sheets. Therefore in this work, Polypropylene SG-170 (PP) sheets of 0.3mm thickness were chosen to investigate the formability and the bending characteristics of the scored groove in respect to the folding direction and residual indentation depth.

2. Experimental method

Figure 1 shows schematics of experimental apparatus for scoring on a 0.3mm thickness PP sheet. In the experimental apparatus, a facet blade (two-line wedge) mounted on the upper crosshead moved downward with the feed velocity V=0.03 mms^{-1}. The two-line wedge was composed of the first (apex) angle α=90° and the secondary α'=30°. Here, a height of the first facet h was 0.15 mm. The wedge blade was made of cemented carbide (FM10K) and it had a tip thickness of 0.8 μm, height of 9 mm, length of 30 mm, thickness of 0.9 mm and the surface roughness Ra=0.09 μm (as a grinding surface).

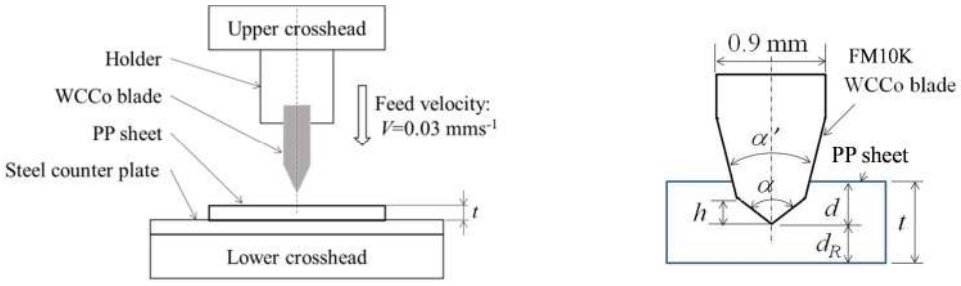

(a) Layout of experimental apparatus

(b) Details of blade profile and definition of d, d_R, h, α, α'

Fig. 1 Schematics of experimental apparatus for scoring

In general, since there is an equivalent-spring effect on the blade displacement, the indentation depth d can be principally estimated with the difference between the blade displacement and device elongation. In this work, the device elongation was not inspected. Alternatively, the indentation depth of wedge blade $d= t–d_R$ was calculated from the measured residual thickness d_R after half cutting (scoring). The applied pushing force F was measured by a load cell.

The PP sheet was a rectangular specimen with a length of 50 mm and width of 15 mm. The position of the blade was vertical to the worksheet, while the angle ϕ of the cutting line direction with respect to Machine direction (MD) of the worksheet was chosen as ϕ=90°.

Table 1 In-plane mechanical properties of PP

Young's Modulus E / GPa	Yield Stress σ_Y / MPa	Tensile Strength σ_B / MPa	Breaking Strain ε_B / -
2.09	23.26	222.40	1.76

Before indenting the blade to, the worksheet was gently placed on the counter plate without any fixture. The depth of wedge indentation was considered as a half cutting condition: $d/t= 1–d_R/t$ = 0.5~0.95. Regarding a shallow indentation of the wedge blade, when $0<d/t<0.4$, due to a low bending stiffness of PP sheet and its large tensile strength, the folding of scored zone behaved unsuccessfully. Therefore, the shallow indentation of wedge blade was not considered in this work. Here, the folding test was carried out using a bending strength tester CST-J1 [11] explained in the below. Table 1 shows the

in-plane mechanical properties of the PP sheet. Here, the strain rate of feeding was chosen as 0.1 s^{-1}. Comparing the mechanical properties between the PP sheet and the reported PET sheet [6], the ratio of the Young's modulus, yield stress, tensile strength and breaking strain were as follows: the ratio of $E._{PP}/E_{PET}$ = 0.92, the ratio of $\sigma_{Y.PP}/\sigma_{Y.PET}$ = 0.33, the ratio of $\sigma_{B.PP}/\sigma_{B.PET}$ =1.47 and the ratio of $\varepsilon_{B.PP}/\varepsilon_{B.PET}$ = 1.48. Namely, the PP sheet is easily flown out but difficult to be broken out, compared to the PET sheet.

The scored PP sheet was bent in either the normal or reverse direction using a crease strength testing machine CST-J1 [11] for measuring the bending moment per unit width M N and the rotation angle θ° as shown in Fig. 2. The distance between the load cell and the scored position (the center of rotation) was set for L=10mm. The scoring and folding experiments were carried out under the following conditions: room temperature of 297 K, room humidity of 50 %RH.

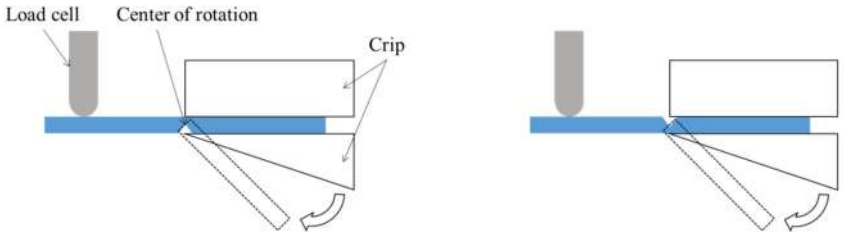

(a) Normal bending (b) Reverse bending

Fig. 2 Schematics of folding test of scored sheet

The work sheet was bent in either the normal or reverse direction with rotation velocity of ω=0.1 rps (revolution per second). Here, the rotation angle θ was repeatedly (twice) varied from zero up to the right angle (0~90°). Figure 3 (a) and (b) illustrate representative response models of relationship between the bending moment resistance M and the rotation angle θ for the normal wise and reverse wise, respectively.

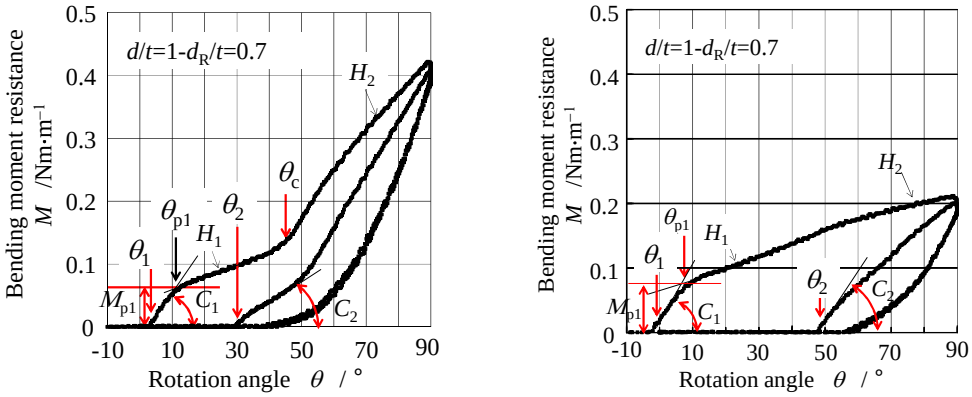

(a) Normal bending (b) Reverse bending

Fig. 3 Response model of bending moment diagram and parameters for characterizing its response.

Through the bending moment response, the first break or inflection bending moment M_{p1}, its corresponded angle θ_{p1}, the first gradient C_1, the second gradient C_2, the initial starting position (angle) θ_1, the second starting position (angle) θ_2, and the two kinds of work hardening gradient H_1, H_2 were measured when varying the indentation depth 1−d_R/t for the normal and the reverse wise bend-

ing. The number of samples was five pieces for each case. Here, in the case of normal wise bending, the gradient H_1 was estimated as the average gradient between the first break point M_{p1} and the starting point of interference, while the gradient H_2 was estimated as that between the middle point of 75° and the tracking (the maximum) position of θ=90°. In the case of reverse wise bending, empirically choosing the middle position as θ=60°, the gradient H_1 was estimated between the M_{p1} and the middle point of 60°, while the gradient H_2 was estimated between the middle point of 75° and the tracking position of θ=90°. In the case of normal wise folding, since there was an interference of wedged groove, the interference based bent inflection angle θ_c was recorded.

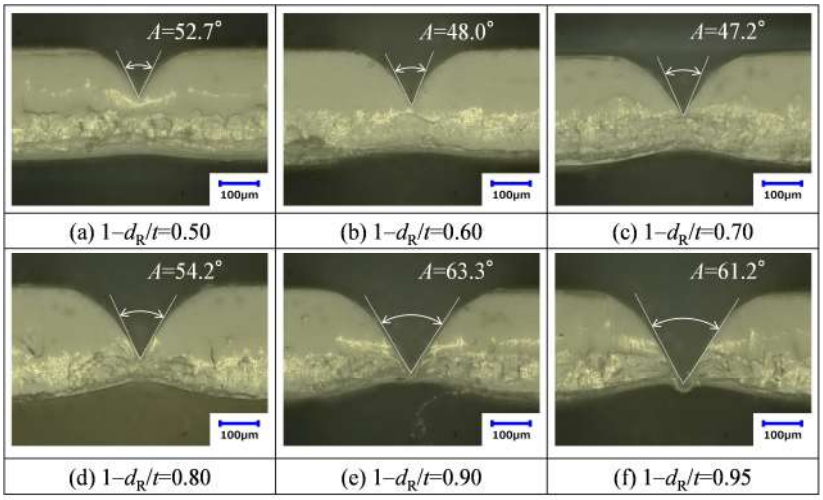

(a) 1−d_R/t=0.50 (b) 1−d_R/t=0.60 (c) 1−d_R/t=0.70

(d) 1−d_R/t=0.80 (e) 1−d_R/t=0.90 (f) 1−d_R/t=0.95

Fig. 4 Sectional views of half-cut (scored) zone of PP sheet

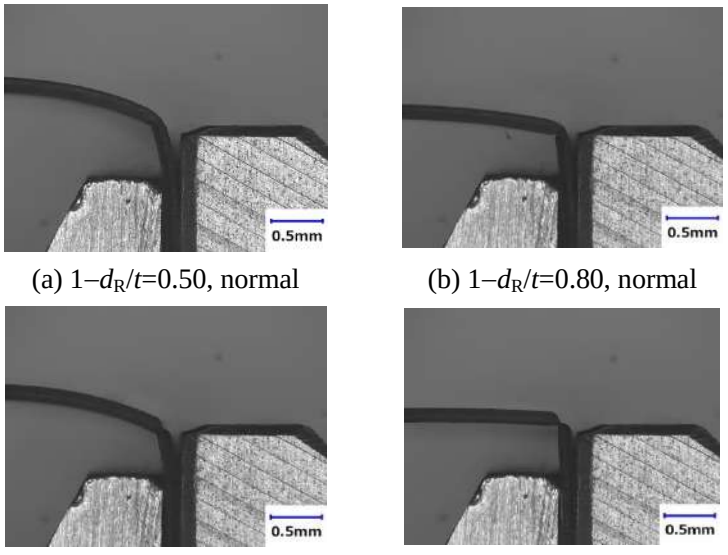

(a) 1−d_R/t=0.50, normal (b) 1−d_R/t=0.80, normal

(c) 1−d_R/t=0.50, reverse (d) 1−d_R/t=0.80, reverse

Fig. 5 Side views of scored PP sheet when folding up to θ = 90 °

3. Experimental results and discussion

Figure 4 shows photographs of sectional views after scoring with 1−d_R/t= 0.50~0.80. The residual (permanent) wedged angle A was measured from those photographs. The value of A was discussed later with the interference resistance during the folding test. Figure 5 shows some photo-

graphs of the scored PP sheets when the worksheets were bent in either the normal or reverse direction with the right angle $\theta = 90°$. Depending on the scored depth, the profile of scored part (groove) was remarkably altered. Figure 6 showed the first break moment M_{p1} with respect to the normal and reverse bending direction. The relationship between M_{p1} and $1–d_R/t$ and that of θ_{p1} were linearly approximated as Eq.(1)-Eq.(4) for the normal and reverse directions.

$M_{p1} = 0.41–0.47\ (1–d_R/t)$ (for normal) (1), $M_{p1} = 0.40–0.47\ (1–d_R/t)$ (for reverse) (2)

$\theta_{p1} = 26.5–22.0\ (1–d_R/t)$ (for normal) (3), $\theta_{p1} = 27.2–24.9\ (1–d_R/t)$ (for reverse) (4)

Comparing the first break (or peak maximum) of M_{p1} of PET [11], M_{p1} of the PP sheet and Eq.(1),(2) were less than 0.1 times of that of the PET sheet, while θ_{p1} of the PP sheet and Eq.(3),(4) were about a half of that of the PET sheet.

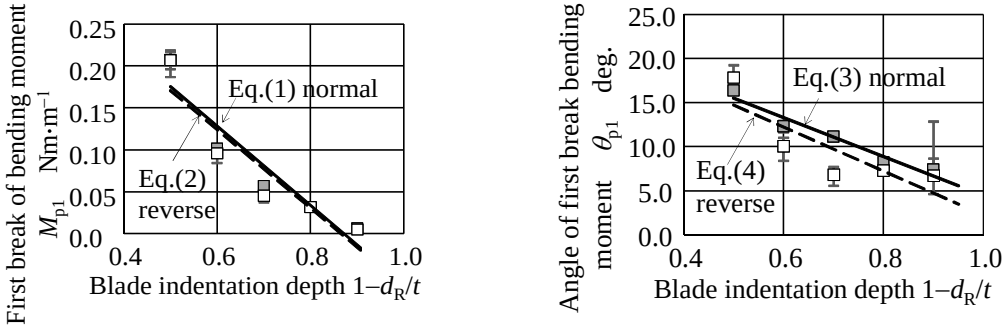

(a) First peak bending moment (b) Angle at first peak bending moment

Fig. 6 Comparison of first peak point with respect to normal and reverse bending

According to the theory of plastically collapse moment with a beam bending [12], the collapse (ultimate) moment per unit width M_{pc} is estimated as $M_{pc} = \sigma_Y \cdot t^2/4 = 0.53$ Nm·m^{-1} when $1\text{-}d_R/t=0$. The nominal collapse (ultimate) moment $M_{pc} = \sigma_Y \cdot {d_R}^2/4$ was estimated as 66~70 % of experimental M_{p1} when $1–d_R/t=0.5$~0.8. This result is a little small but seems to have a primary contribution. Using the yielding stress ratio $\sigma_{Y.PP}/\sigma_{Y.PET} = 0.33$ and the thickness ratio 0.3/0.5= 0.6, the value of M_{pc} of 0.3mm PP sheet is estimated as 0.11 times of that of 0.5mm PET sheet. It was found that the order of collapse moment matched to the range of the first break (or peak maximum) bending moment when varying the indentation depth of $1–d_R/t$. Here, since the ratio of Young's modulus of PP by PET was $E_{.PP}/E_{PET} = 0.92$, the strain for starting the yield seems to have the same order as that of $\sigma_{Y.PP}/\sigma_{Y.PET}=0.33$. Since the ratio of θ_{1p} for both cases was about 0.5, the yield ratio of 0.33 was not equal to this break angle ratio, but they were related with each other.

Figure 7 shows a representative relationship between M and θ when varying the indentation depth of blade. The interference of scored groove occurred in the normal wise bending. As the result, a remarkable increase of bending moment M was detected. Through the results of relationship between M and θ, the gradients of C_1, H_1 , H_2 and C_2 were arranged with $1–d_R/t$. The first starting angle θ_1 was almost zero for all the cases in this work.

Figure 8 shows the first gradient C_1 and second gradient C_2 of bending moment resistance with respect to the normal and reverse bending direction. In the case of the normal folding, C_1 and C_2

were linearly approximated with $1-d_R/t$ as Eq.(5), Eq.(6). Here, the relation of $0<C_2<C_1$ seems to be caused by damages of folding repetition. It was found that C_1 of the normal bending was almost same as that of the reverse bending, and also C_2 was similar between the normal and reverse bending. The ratio of C_1, C_2 between PP and PET [6] was about 0.13~0.19 at c/t=0.5. Since the first gradient C_1 is approximately expressed as M_{p1}/θ_{p1}, the values of C_1, C_2 seem to be strongly affected by the yield stress of the worksheet and the residual thickness d_R.

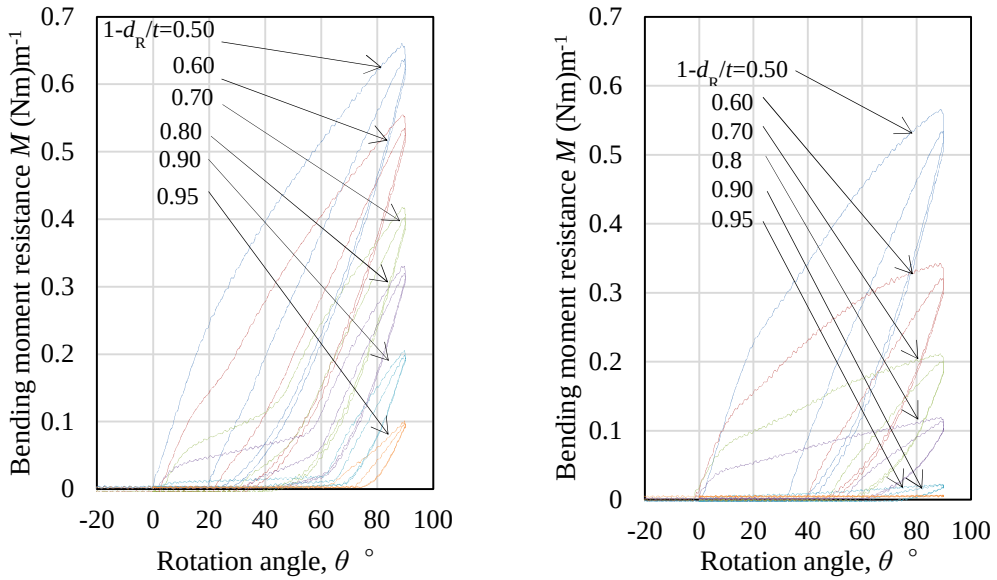

Fig. 7 Relationship between bending moment resistance and rotation angle when varying indentation depth of blade.

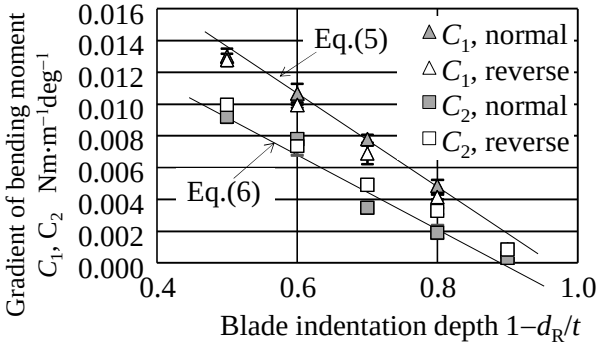

Fig. 8 Relationship between first and second gradients of bending moment and indentation depth of blade, along with normal and reverse bending modes.

$$C_1 = 0.029-0.03(1-d_R/t) \approx 0.03 d_R/t \quad \text{(for normal)} \tag{5}$$

$$C_2 = 0.021-0.023(1-d_R/t) \approx 0.02 d_R/t \quad \text{(for normal)} \tag{6}$$

Fig. 9 (a) shows the first half gradient of bending moment H_1, while Fig. 9 (b) shows the second half gradient of bending moment H_2 with the normal and reverse bending. The difference of the latter gradient H_2 between the normal and reverse bending were obviously caused by the groove interference of normal bending. There is a small difference in the H_1 for $1-d_R/t \leq 0.6$. It seems to be caused by the interference behavior in the groove. In order to discuss this problem, the bent inflec-

tion angle θ_c and wedged angle A were shown in Fig.10. Here, the plotted data were evaluated from the average and the representative photograph. The value of θ_c was almost equal to that of A, namely the initial clearance of groove was sufficiently kept when $1-d_R/t \geq 0.7$. In case of shallow blade indentation, the wedged groove clearance is insufficient and the bent inflection of θ_c becomes invisible. When the groove depth is the deeper, the difference of H_1 between the normal and reverse bending becomes elastic deformation without interference and similar with each other. In the case of PET sheet, the wedged angle A was relatively larger than that of PP sheet. For an example, A= 84 degrees when $1-d_R/t$=0.57 [6].

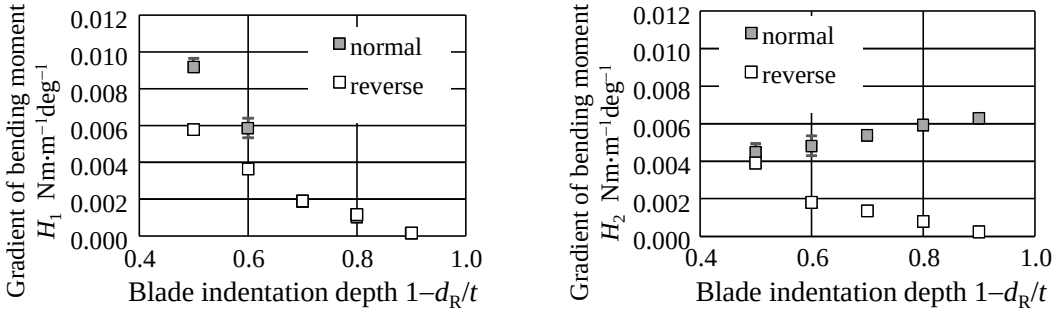

(a) First half gradient H_1 (b) Second half gradient H_2

Fig. 9 Anaphase characteristics of bending moment

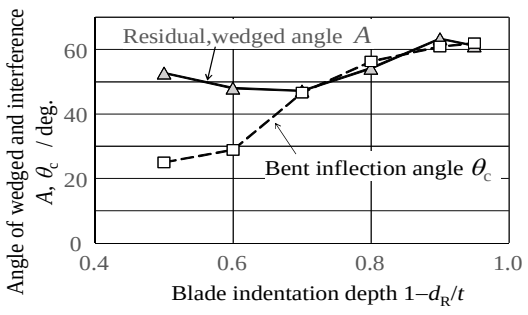

Fig.10 Wedged angle and inflected-bent position

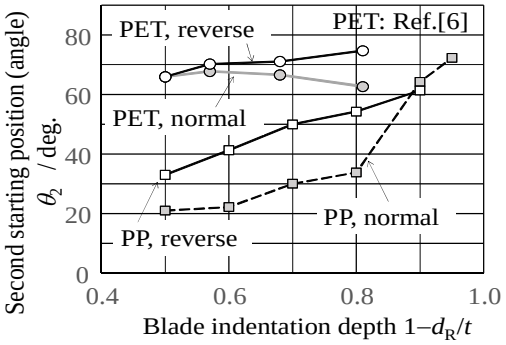

Fig.11 Second starting position (angle)

Regarding the repeated (as twice folding) elastic behavior, the second gradient C_2 and the second starting position θ_2 were investigated. Figure 11 shows the comparison of θ_2 with the normal and reverse folding, along with that of PET [6]. Here, the graph was derived from the average for each case. Seeing Eq.(5),(6), C_2 was about 67% of C_1. This relation was almost the same level with the normal and reverse folding. Seeing Fig.11, it was found that θ_2 was remarkably affected by the folding direction (normal and/or reverse) in the case of PP sheet for $1-d_R/t \leq 0.8$. When choosing $1-d_R/t \geq 0.9$ in the case of PP sheet, the value of θ_2 was 60-70 degrees (67~78% of 90 degrees), which was almost the same as that of PET sheet.

4. Conclusions

In order to detect allowance of mechanical conditions of two-line wedge blade, the crease characteristics of polypropylene sheets of t= 0.3 mm thickness were investigated. Regarding the normal

and reverse bending of scored part, the bending characteristics such as the first/second stiffness gradient C_1, C_2, the first/second work hardening gradient H_1, H_2, the first break (or peak maximum) bending moment M_{p1}, and its corresponded angle of θ_{p1} were experimentally investigated with respect to the indentation depth of blade. Some of them were compared with that of PET sheet. Through this experiment, the following results were revealed.

1) Bending stiffness parameters such as C_1, C_2, M_{p1}, θ_{p1} were characterized with the yielding stress σ_Y and the residual thickness d_R. They were strongly related to the plastic collapse moment.

2) The profile of wedged groove was different from that of PET sheet, when using the same tip shape of two-line wedge blade as for $0.5< 1-d_R/t <0.95$. Depending on the wedged angle A, in the case of the normal folding, a bent inflection point of bending moment occurred at the rotation angle $\theta_c \approx A$ for $1-d_R/t \geq 0.7$.

3) Regarding the repetition (twice folding), the relationship between the second starting angle θ_2 and the residual thickness d_R was different from that of PET sheet. It tends to be similar to that of PET sheet for the range of $1-d_R/t >0.9$.

When choosing $0.5<1-d_R/t <0.8$, the tip profile of the wedge blade is ought to be changed and its scoring characteristic should be investigated furthermore.

References

[1] R.J. Crawford, Plastics Engineering, 3 eds., Burlington: Elsevier Butterworth-Heinemann, (1999), pp.1-40.

[2] Japan Society for Technology of Plasticity eds., in: Processing Technology of Plastics, Bending, (2016), pp.229-230 (in Japanese).

[3] Tadashi Hashimoto, Processing Technology of Transparent Packaging Box and Related Problems, CARTON-BOX, vol.23 (2004), pp.44-45 (in Japanese).

[4] F. Hesse, H.J. Tenzer, Grundlagen der Papier-verarbeitung, VEB Verlag fur Buch und Biblio-thekswesen, Leipzig, (1963), pp. 58-60 (in Germany).

[5] S. Mizuguchi, eds, Advanced Technology on Industrial Packaging and Transportation, Fuji Techno System, Tokyo, (2002), pp. 58-59 (in Japanese).

[6] Shigeru Nagasawa, Kiminori Sato, Mitushiro Murayama, Yasushi Fukuzawa, Effect of Tool Condition on Bending Characteristics of Polyethylene Terephthalate Board Subjected to Two-Line Wedge Indentation, Proceedings of the 10th International conference on technology of plasticity (ICTP 2011), Aachen, Germany, pp.984-989.

[7] Shigeru Nagasawa, Cutting and Bending of Plastics Sheet, Journal of Japan Society for Technology of Plastics, vol.57 no.665 (2016), pp.867-872 (in Japanese).

[8] Hideaki Ishihara, Fundamental and Application of Plastics Films, Converting Technical Institute, Tokyo, (2010), pp.33-52 (in Japanese).

[9] Satoshi Okuda, Woo Sik Choi, Mechanism of Cutting Fracture of Polypropylene by Impact on Wedge-shaped Target, Journal of Chemical Engineering of Japan, vol.14 no.2 (1981), pp.149-153.

[10] W. Bauer, D. Wustenberg, Fracture Behavior of Polypropylene under Dynamic Cutting and Shearing Action in Granulators, Chemical Engineering and Technology, vol.25 no.11, (2002), pp.1047-1051.

[11] Katayama Steel Rule Die Inc., “Crease Stress Tester CST-J-1”, (accessed on September, 2016), http://diemex.com/sale/cst.html.
[12] Hideaki Kudo, Plasticity, Morikita publishing, Tokyo, (1968), pp.16-19 (in Japanese).

(Received: 10 October 2016, Accepted: 17 February 2017)

Improvement to Reduce Delay Time in Transportation to Disaster Area using Similarity to Electric Circuit

Chata Yorvarak[1, a], Thanat Rungsirathana[2], Kazumasa Takahashi[1], Toru Sasaki[1], Takashi Kikuchi[3], and Nob. Harada[1]

[1)]Dept. Electrical, Electronic and Information Technology, Nagaoka University of Technology,
[2)]School of Engineering, University of the Thai Chamber of Commerce,
[3)] Dept. Nuclear System Safety Engineering, Nagaoka University of Technology,
1603-1 Kamitomioka-machi, Nagaoka 940-2188, Japan
**E-mail: yorvarak026@gmail.com, nob@nagaokaut.ac.jp*

Transportation is closely related to many sectors such as economic, political and social environment of the country. It is necessary to identify suitable transportation method for keep the pace of the country's economy and life style of citizens in disaster times. Currently most frequent disaster in the world is flooding and this study focused to reduce the delay time in transportation for those crisis to sending disaster reliefs. Similarity between the logistics and electrical circuits will be used to stimulate the transportation models which can be used in disaster times. Simulation work in this study was carried in this study using the MATLAB/Simulink software and parameters were introduced to system considering the similarity between logistics and electrical circuits. Initially study focused on water distribution to disaster areas in chaos time where parameters such as amount of water required were identify as amount of charge in electrical circuits for the simulation. Also requirement of number of tucks for the delivery was identified as number of pulses in electrical circuit and capacity of water storages were identified as capacitance of the electrical system, etc. Centralized distribution model was stimulating for understanding the behaviors of the electrical charge flow and change of parameters which are similar to electrical circuit shows changes in the flow of charges with time in the electrical circuits which can be adopted to logistic patterns. Present study results show decentralized patterns is more suitable than the centralized patterns for improve to reduce the delay time in transportation in disaster areas.

1. Introduction

A disaster incident is defined as incident of any natural or man-made, that result in levels of serious damages to human, properties, economic or environmental losses which affecting the people directly [1]. Disaster occurrence have increased significantly in last several years in many countries, in that flood disaster has the highest occurrence frequency among all natural disasters. It is necessary to have a plan to flow model to help decide how to rapidly supply aid to victims of a disaster within this context [2]. Include find the optimization route to suitable in these situations because reservation others alternative can find the optimize route to supply as soon as possible for respond people who are in disaster. The main purpose is to provide a faster response, possibly by decreasing delay time between the origin and destination of supplies. We propose an optimization model that could be used within a decision-aid tool are currently responsible for providing rapid responses in disaster relief. However, logistic can offer lots of logistic patterns and it is essential to identify and stated proper logistic plan to send relief items to disaster areas. In these situations, disaster relief logistics (DRL) can be applied [2], [3].

When using DRL and developing logistic systems, it is necessary to understand the processes and pathways of that plan. Using electrical circuit can be helpful to run and tested the models before goes for the actual logistic plan. Through the concepts of the electrical circuits, with the similarity with logistics, can tested the different scenarios of the disaster and can identify the most suitable plan for the cause. For testing logistic plans through electric circuits can be stimulate through different software programs and it will reduce the collection of huge amount of data and testing time of the

logistic plans. MATLAB/Simulink is one of the powerful applications to stimulate electrical circuits for optimization, statistics, mathematical functions, or data analysis, then there is a very quick learning curve for using it in image processing. This study focused on optimization model for find the best way to quickly respond to disaster victims because of the situation is often unclear in the immediate aftermath of the disaster. The option of a route that can respond most and to identify the similarity between the logistic and electrical circuits and stimulate developed electrical circuit models to identify the suitable logistic patterns to assess the logistic models for disaster reliefs.

2. System Parameters and Modelling

Proper logistic network can reduce the delivery time and also the cost of distribution reliefs in disaster time. However, in this study electrical circuits will be analyzed using the MATLAB/Simulink software and it requires to introduce proper parameters for analysis. Fig. 1 shows the simple concept for logistic model to deliver water to disaster area point "1" from the distribution center/warehouse which is point "0". Introduced electrical circuit network for the logistic model is shown in the Fig. 2 and Table 1 shows the relation between the logistic and electrical circuit with set parameters for evaluation. For the evaluation model water can be considered to be electric charge.

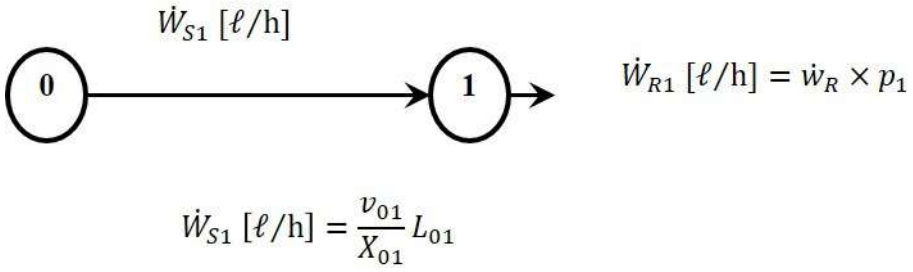

Fig. 1 Basic logistic model from the point "0" to the destination point "1".

Table 1 Similarity relation between logistic and electric circuit for the case of water supply.

	Logistics	Electric Circuit
Required water for a man	$w_R \left[\frac{l}{h}.man\right]$	$I_{S1}\ [\mathrm{C/s}] \equiv I_{S1}[\mathrm{A}]$
Population in certain disaster area	P_1	P_1
Supply speed of water	$W_{S1}\ [l/h]$	$I_{S1}\ [A] \equiv Q_{S1}[\mathrm{C/s}]$
Distance between nodes	$X_{01}\ [km]$	R_1
Speed of carrier	$V_{01}\ [Km/h]$	V_1
Capacity of the carrier (per hour)	$L_{01}\ [l]$	C_1

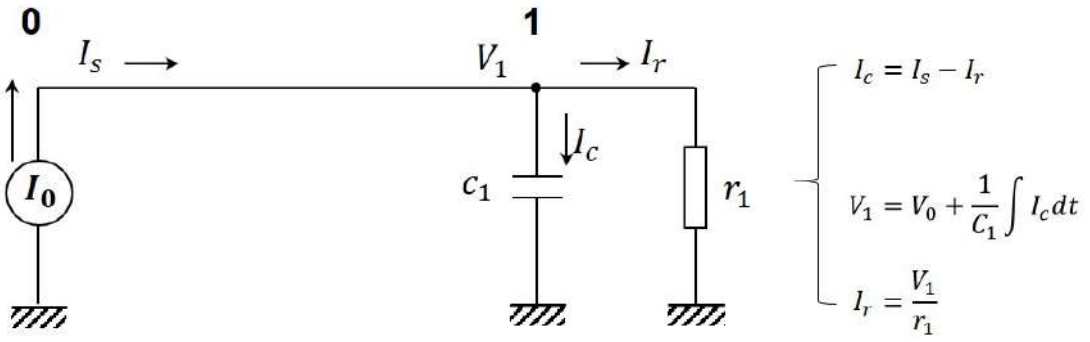

Fig. 2 Logistic equivalent electrical circuit for the simple logistic model for water delivery model.

3. Assumptions-water supply/current source

Typical source of water delivery is shown in Fig. 4 where 6 trucks with each capacity of 4000L. So it looks like rectangular pulse series as shown in Fig. 4.

Fig. 4 Assumed for source storage.

For the simulation water supply will be consider as a digital pulse with a delay time which was calculated using the assign parameters of distance between two nodes and speed of truck. For the analysis of the two scenarios which are 1. Storage without any initial items and 2. Storage with initial amount of items were considered

4. Analysis of Electrical Circuit using Simulink Model

4.1 Basic Model

The model for a logistics using electrical circuit was created by using MATLAB/Simulink software as shown in Fig. 5. The process of connection between the blocks-cells and flow between each block created through Simulink. For analysis, two models were created where the Model 1 concidering *no initial storage* and the Model 2 with 50% of *initial storage*. Simulink model was created using the components of its library and parameters were defiend in the property boxes of each component.

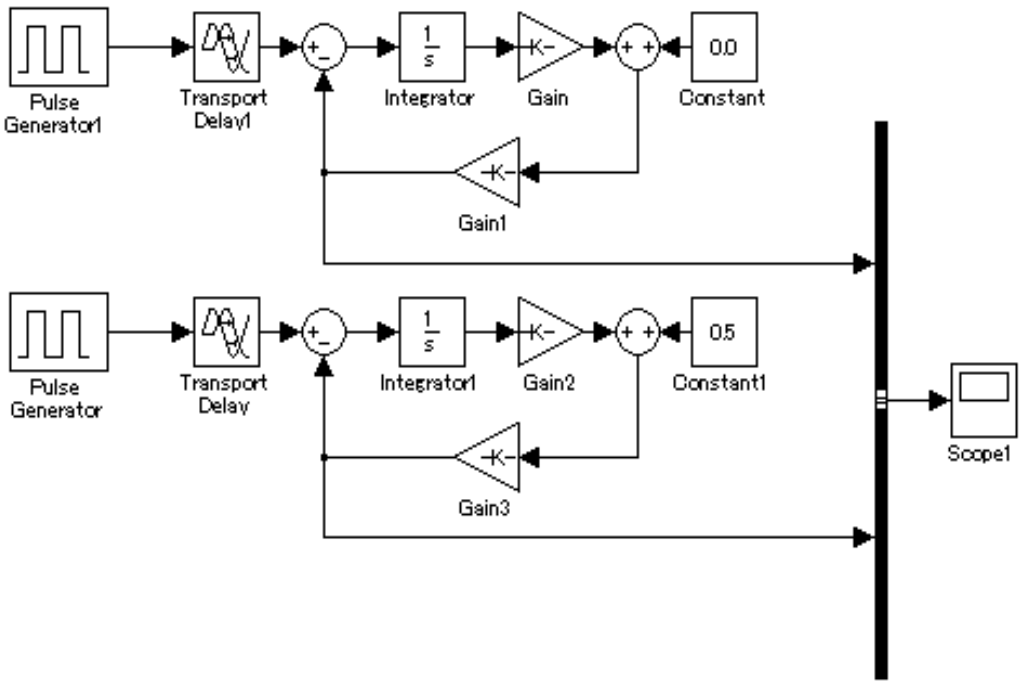

Fig. 5 Basic logistic model created using MATLAB/Simulink.

4.2 Assigning Values for Simulation

Primary values were assigned as shown in the Table 2 for run the basic analysis of the two models and relevant platform were used to assign values to the program for simulation. In this simulation program one liter were considered to be one micro coulomb (1 l = 1 μC) and one hour to be one second (1 h = 1 s). Typical simulation results for these models were shown in Fig. 6. We could see that initial delay of water supply for the both cases but in black curve (Model 1) there is a crisis without the water till receive its first batch of water. On the other hand, red curve (Model 2) shows that water can be supplied from initial storage till receive its initial water supply. Rate of supplying water was considered as the function of water in the tank and results shows with higher storage of water can help to increase the supply rate for disaster victims.

Table 2 Assigned parameters

Parameter	Model 1	Model 2
Number of trucks	8	6
Truck capacity (million liters)	0.025	0.025
Distance (km)	450	600
Truck speed (km/h)	65	65
Storage of tank (million liters)	0.6	0.6
Initial storage (million liters)	0.0	0.05

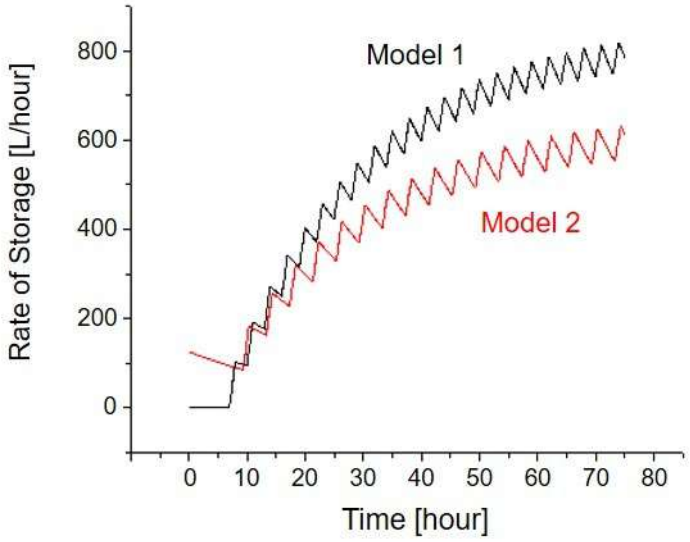

Fig. 6 Simulation results for the Model 1 and Model 2.

4.3 Changes in parameters

4.3.1 Same set of parameters values for both models

Fig.7. shows that the frequency of both curves were same and the delay time also same as the input parameters are similar to each other. However, for the result 2 which had initial storage (red curve) always went over the result 1 (black curve) as its storage facility contained more relief items every time, comparing to both cases. The distribution rates somewhat different compare to each other as red curve to black curve as the result 2 had more initial storage.

4.3.2 Change in distance between point 0 and point 1

Change in the parameter of distance between distribution point and disaster point showed how it affected the delay time for distribute relief from point 0 to point 1. Longer distance in the result 2 compare to that in the result 1 caused larger delay time which was shown in Fig. 8. As other parameters were the same, frequency should be the same between two nodes.

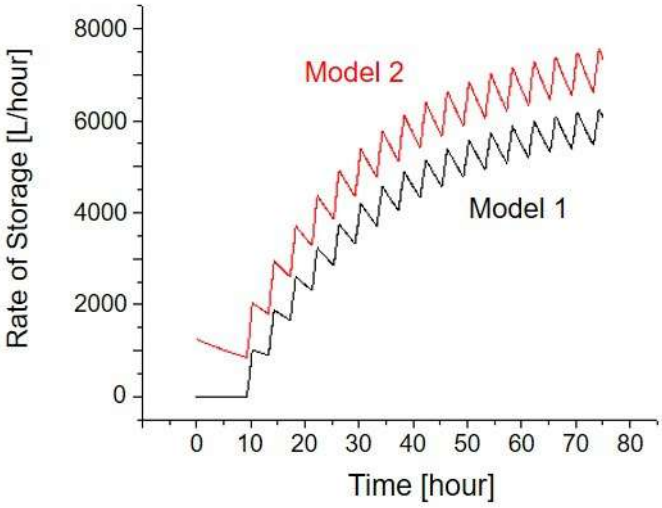

Fig. 7 Evaluation for same parameters (black curve - result 1, red curve - result 2).

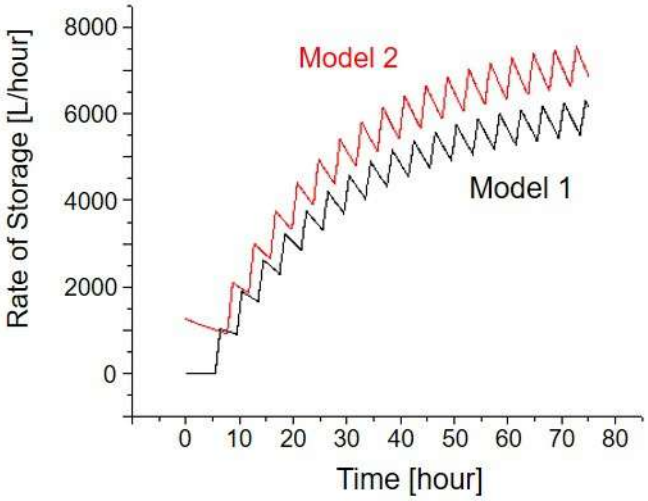

Fig. 8 Evaluation for change in distance (black curve - result 1, red curve - result 2).

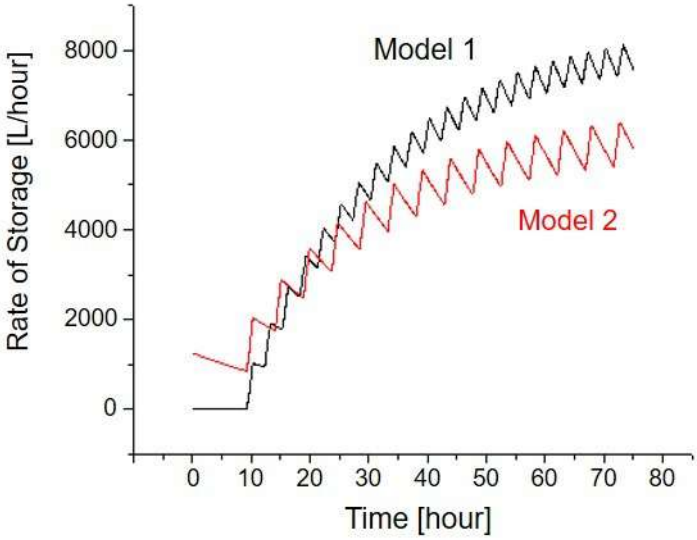

Fig. 9 Evaluation for change in number of delivery trucks.
(black curve - result 1, red curve - result 2)

4.3.3 Change in number of delivery trucks

Influence of change in number of trucks on the delivery curves was shown in Fig.9 as no storage situation overcome the initial storage as the number of trucks bringing more capacity of the disaster reliefs per a day in the result 1 compare to that in the result 2. As other factors were kept constant frequency dependence could be important point in disaster area which need higher priority.

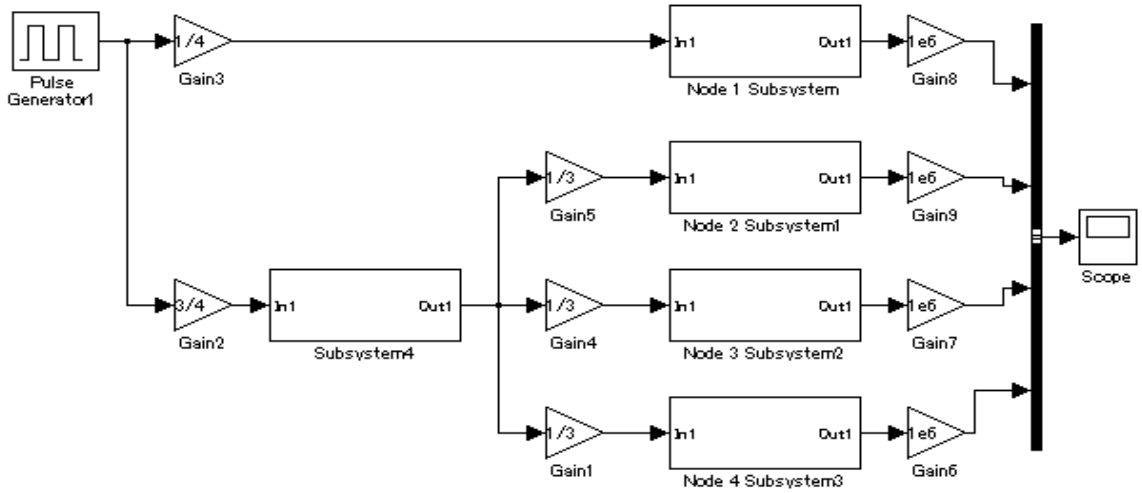

Fig. 10 Proposed model for reduce delay time in disaster relief transportation.

Conclusion

Logistic related electric circuits are relatively easy for analyzing through the simulation than the real time data collection and analysis. This study was carried out with MATLAB/Simulink simulate software as it provides easy platform for analysis and it helps to make variation for the possible real time scenarios. For the preliminary results, it was observed that the amount of water supply per a day had an impact as how much relief could be sent at disaster time. When sending the disaster relief items, longer the distance increased the delay time of delivery, and therefore, initial capacity tank and/or initial storage of the disaster areas played a major role in addressing the disasters as soon as possible. So, in this study we were recommended to have another sub-terminal between main distribution points to disaster area as show in Fig.10. and built some storage or tank to keep initial storage for distribute relief items till the enough relief items coming from distribution centers.in order to reduce delay time. both the closer distribution point and the larger initial storage could increase the more delivery of disaster relief items.

References

[1] Mei-Shiang Chang, Ya-Ling Tseng, Jing-Wen Chen, "A Scenarioplanning approach fo the flod emergency logistics preparation problemm under uncertainty," *Transportation Research* , vol. 43, no. E, pp. 737-754, 2007.

[2] A. Thomas & M. Mizushima, "Logistic Training: necessity or luxury?. Forced Migration Review," Fitz Institute, 2005.

[3] Mohammad Rezaei-Malek, Reza Tavakkoli-Moghaddam, Behzad Zahin, Ali Bozorgi-Amiri, "An interactive approach for designing a robust disaster relef logistics network with perishable commodities," *Computers & Industrial Engineering*, vol. 94, pp. 201-215, 2016.

(Received: 7 October 2016, Accepted: 2 December 2016)

An Observation on Potential Alkali Silica Reactivity of Natural Aggregate in Myanmar

Pyae Phyo Kyaw[1], Thynn Thynn Htut[2,*]
[1)]Quality Control Department, Tetlann Concrete Co., Ltd.,
[2)]Building Department, Taisei Myanmar Co., Ltd.
No. 32, The Tokyo Enterprise Building, 6 ½ Mile, Hlaing Tsp, Yangon, Myanmar
**E-mail: thynnhtut@taiseimyanmar.com*

Most aggregate used in concrete are almost chemically inactive, however, mineral constituents of some aggregates react with alkali hydroxide, which originates mainly from the Portland cement. The chemical reaction, internally occurred alkali–silica reaction (ASR) in either concrete or mortar under a certain condition, e.g. high humidity and sea saline water, may result deleterious expansion of concrete or mortar. The prior evaluation of alkali-aggregate reactivity by the reliable test is required for the utilization of natural aggregate in concrete for assurance on the longer service life of the structures.

The objective of this study is to identify the potential alkali–silica reactivity of several aggregates which able to buy in Yangon region, Myanmar. To achieve this objective, four numbers of fine aggregate quarry which are operated to produce river sand was selected and investigated. In addition, three numbers of coarse aggregate quarries were also chosen to investigate potential alkali–silica reactivity.

Four samples of river sand, one sample of river shingle and three samples of crush stone were collected from the mentioned quarries and the accelerated Bar Mortar test was conducted on these samples to assess the potential alkali–silica reactivity. According to ASTM C 1260 suggested method, three Bar Mortar tests were performed on each sample. Based on the obtained results, it was found that four samples of all seven samples were considered as non-reactive due to their average expansion rates which are less than 0.1%. Two samples which were collected from Wan Be Inn and Ohn Chaw quarry are considered as moderately reactive which average expansion rate between 0.1% and 0.2%. Only one sample taken from Kamaryut quarry is concluded as reactive with the average expansion rate of 0.3429% which is more than 0.2%.

1. Introduction

Generally, alkali–silica reaction (ASR) is considered as an internal chemical reaction between the alkaline components in the cement and active silica–silicate based mineral constituents of some aggregates. The use of aggregates susceptible of ASR in concrete can cause severe degradation of the concrete structures because of several reasons e.g. high humidity and sea saline water [1]. Map-like cracks appear when concrete is suffered from ASR [2]. Many researchers have stated that ASR is generated due to combine action of existence of a significant quantity of reactive silica in aggregates, having critical level of alkalis (sodium and potassium) in pore solution of concrete and water or moisture from the external source. Utilization of potentially alkali–silica reactive aggregates needs to conduct reliable tests for evaluating their alkali–silica reactivity [3,4].

Generally, it is considered that aggregates from the quarries in Yangon area are not reactive. The portion of aggregate quarry which may have potential reactive aggregates need to be identified. Hence, the research study undertaken has following aims and objectives:

- To identify the potential alkali–silica reactivity of several aggregates available in Yangon region, Myanmar

- To identify Coarse aggregate which meets criteria of AASHTO.

To achieve this objective, four numbers of the fine aggregate quarry which is operated to produce river sand was selected to investigate alkali–silica reactivity of sand. In addition, three numbers of the coarse aggregate quarry were also chosen for the same purpose. Aggregate samples are collected from the mentioned quarry and an extensive laboratory tests: accelerated Bar Mortar test was conducted on these samples to assess the potential alkali–silica reactivity.

2. Evaluation of Alkali-Silica Reactivity

2.1 Fine and Coarse Aggregate Quarry

The selected quarries for evaluation of alkali-silica reactivity of aggregate are listed in Table 1. The aggregate manufactured from those quarries are mainly supplied to the construction industry in Yangon region.

Table 1 List of sand and coarse aggregate quarry

Sr. No	Quarry Name	Material	Name of River	Region	Township
1	Wartayar	River sand	Hlaing River	Yangon	Shwe Pyi Thar
2	Thilawa	River sand	Yangon River (Tidal Mouth)	Yangon	Thanlyin
3	Kamayut	River sand	Yangon River	Yangon	Kamayut
4	Wan Be Inn	River sand	Sittaung River	Mon state	Thein Za Yat
5	Mi Kyaung Ye	River shingle	Ayeyarwaddy	Bago	Pyay
6	Ohn Chaw	Crush stone	-	Mandalay	Ohn Chaw
7	Moke Pa Lin	Crush stone	-	Mon state	Moke Pa Lin

2.2 Sample Collection

Fig 1 Aggregate Samples

The aggregate samples are collected from the quarry stated in Table 1 and those samples are shown in Fig 1. The coarse aggregate is crushed and the crushed aggregate is poured onto the sieves to separate them into their various sizes. Then it is washed each size with a water spray over the sieve to remove adhering dust and fine particles from the Aggregate. Each portion is placed into the oven at 105 Degree Celsius and allows to dry overnight. Each such portion is individually stored in a clean container provided with a tight-fitting cover. Just before casting, the aggregate is combined in the following grading requirements as in table 2 for aggregate with relative density ≥2.45 g/cm^3.

Table 2 Grain Size Distribution for Mortar Bar [5]

Sieve Size		Mass (%)	Mass (g)
Passing	Retained on		
4.75mm	2.36 mm	10	99
2.36mm	1.18 mm	25	247.5
1.18mm	600 µm	25	247.5
600µm	300 µm	25	247.5
300µm	150 µm	15	148.5

2.3 Moulding Mortar Bar

Portland cement that meets the requirements of ASTM Specification C 150 is used. Lumps are removed and cement are passed through an 850 -µm sieve before use. Then, aggregate and cement are mixed in a mixing bowl. The moulds are filled up with two approximately equal layers, each layer being compacted with the tamper. The mortar is placed into the corners, around with gauge studs and along the surface of the moulds with the tamper until a homogeneous specimen is obtained.

2.4 NaOH Solution Preparation

Initially, using a weighing balance with weigh 40g of NaOH pellets and dissolved in 900ml of distilled water. Then, it pours the solution into a 1000ml volumetric flask and fills up the solution to the point with more distilled water.

2.5 Conditioning

The temperature of moulding room and dry materials are maintained between 20 °C and 27.5 °C. Also, the moist room and closet are controlled to be 23°C±1.7°C. The relative humidity of the moulding room is kept at 50%. The specimens are stored in the storage oven that controlled temperature at 80 ± 2 °C.

Fig 2 Mortar Bar Mould

Fig 3 Storage Oven

2.6 Initial Storage and Reading

Each mould is placed in the moist cabinet immediately after moulds have been filled. The specimens are kept in the moulds for 24 ± 2 h. The specimens are removed from the moulds and, while they are being protected from loss of moisture, give the name to specimens and make an initial comparative reading. The initial and all subsequent readings to the nearest 0.002 mm are made and recorded. The specimens are placed in a storage container with sufficient tap water to totally immerse them. The container is sealed and placed in an oven at 80.0 ± 2.0°C (176 ± 3.6°F) for a period of 24 hours. The container is removed from the oven then, the specimens are taken off from the container and the surfaces of mortar bar are dried with a towel paying particular attention to the two metal gage studs. The zero reading of each bar is made immediately after drying and read as soon as the bar is in position. As specified in ASTM C-1260, the process of drying and reading is completed within 15 ± 5s of removing the specimen from the water. After comparative readings on the remainder of the bars, all specimens made with each aggregate sample are placed in a container with sufficient NaOH, at 80.0 ± 2.0°C (176 ± 3.6°F) for the samples to be totally immersed. The container is sealed and returned to the oven. The subsequent comparator readings of the specimens are made periodically, with at least three intermediate readings, for 14 days after the zero reading, at approximately the same time each day.

2.7 Calculation of Percent Expansion

The difference between the zero-comparative reading of the specimen and the reading at each period to the nearest 0.001 % of the effective gage length is calculated and record as the expansion of the specimen for that period. The average expansion of the three specimens of a given cement-aggregate combination to the nearest 0.01 % as the expansion for the combination for a given period is recorded. The expansion (E_n) of each mortar bar from the following equations.

$$E_n = \frac{L_n - L_2}{250} \times 100$$

and, if required, the value of thermal expansion

$$TE = \frac{L_2 - L_1}{250} \times 100$$

E_n = expansion at the time n days, after immersion in the NaOH solution at 80°C in percent [%]
TE = thermal expansion after heating to 80°C in the water bath [%]
Ln = comparator reading at time n days after immersion of mortar bars in the NaOH solution [mm]
L1 = Initial comparator reading [mm]
L2 = comparator reading after heating to 80°C in the water bath [mm]

3. Results and Discussion

3.1 Aggregate Reactivity Classification

Aggregate reactivity is classified based on the 16 days expansion values in accordance with

Table 3, which tabulates the requirements of ASTM standard specification.

Table 3 Aggregate reactivity classification [5]

Mortar Bar Expansion (%) in NaOH (80%)	Classification
Less than 1%	Non-reactive
Less than 2%	Reactive
More than 2%	Moderate reactive
Individual results shall not differ from the mean by more than 15%.	

3.2 Experimental Results

Fig. 3 shows expansion of mortar bar incorporated with fine aggregate from War Ta Yar Quarry. The expansion curves for WTA-1, WTA-2 and WTA-3 are in the same trend. The expansion rates are very small. All specimens have under 0.03 % in the expansion of 16 days.

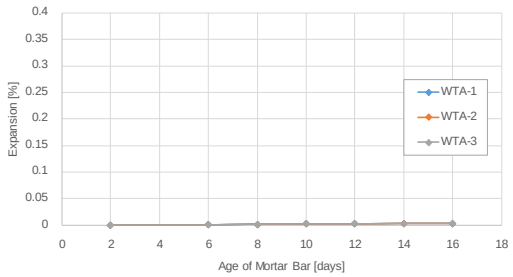

Fig 3 Expansion of mortar bar (Wartayar)

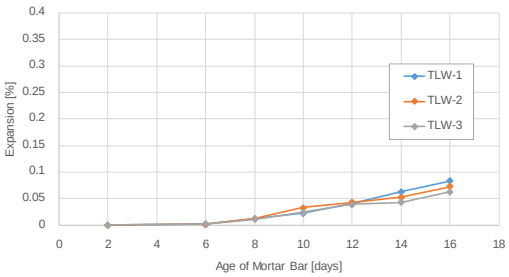

Fig 4 Expansion of mortar bar (Thilawa)

In figure 4, the expansion of mortar bars composed of sand from Thilawar quarry shows small expansion in early of the experiment. Afterward, gently increase in expansion happened started from 6 days till the age of 16 days. The expansion of all specimen at the age 16 days don't reach 1%.

Expansion curves of KMT-1, KMT-2 and KMT-3: sand from Kamaryut quarry incorporated into mortar bars are shown in Fig.5. The sudden increase in expansion found between 10 and 12 days of the experiment. It can be seen in Fig 10 that the average expansion curve for Kamaryut sand pass through a moderately reactive zone and it reached reactive zone at age of 12 days. Then, expansion rates significantly increase until the end of the experiment: the last test for the age of 16 days. It is clear that sand from Kamaryut quarry is the reactive aggregate.

Expansion of specimen by Wan Be Inn aggregate is shown in Fig. 6. Expansion curves for all of the mortar bars: WBL-1, WBL-2 and WBL-3 gradually increase from the beginning of the experiment to test on 12 days. After that moment, the expansion rate doesn't increase and become stable until the end of the experiment.

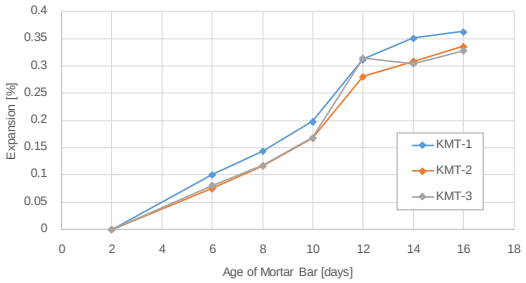

Fig 5 Expansion of mortar bar (Kamayut)

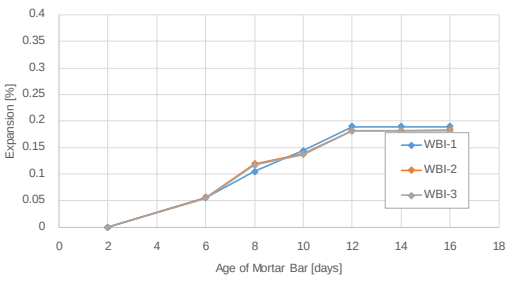

Fig 6 Expansion of mortar bar (Wan Be Inn)

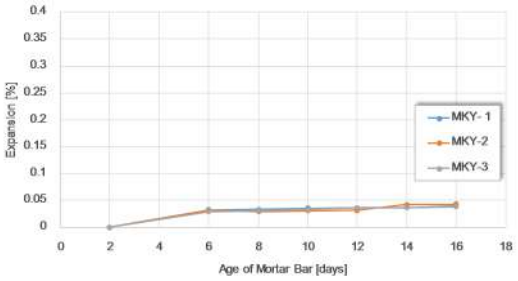

Fig 7 Expansion of mortar bar (Mi Kyaung Ye)

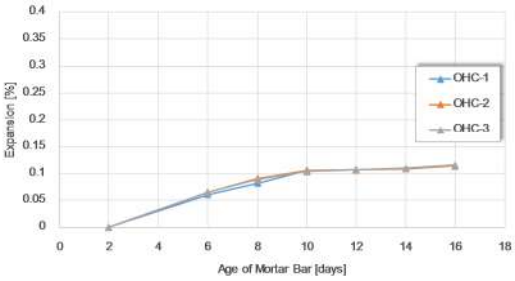

Fig 8 Expansion of mortar bar (Ohn Chaw)

Expansion of mortar bar made with river shingle from Mi Kyaung Ye quarry is shown in Fig 7. Expansion % at the age of 6 days slightly grow up for all mortar bar reach 0.03% expansion. At the age 10 and 12, all specimen exhibit expansion and MKY-1 and MKY-3 reach 0.035% expansion. Afterward, MKY-02 has the great increase in expansion at the age of 14 days and it subsequently goes stable at the end of the experiment: 16 days in age of mortar bar. The tendency of expansion curves for all: MKY-1, MKY-2 and MKY-3 are the same. It can be said that the results are reliable.

Expansion of mortar bar made up of aggregate from Ohn Chaw Quarry is displayed in Fig.8. In its experiment, all mortar bar: OHC-1, OHC-2, and OHC-3 are in the same tendency in expansion from the beginning of experiment till the end of the experiment.

As shown in Fig. 9, expansion % of mortar made up of sand from Moke Pa Lin quarry increase with a great extent until the age of 8 days counted from the start of the experiment. The highest expansion % of MPL-3 is 0.045% at the age of 16 days and the others are 0.04% at the same age.

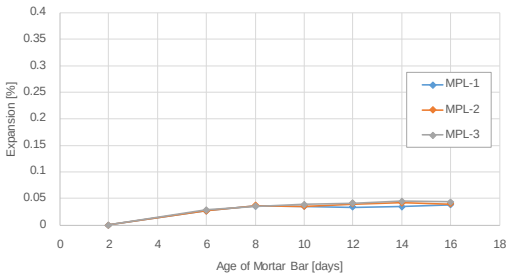

Fig 9 Expansion of mortar bar (Moke Pa Lin)

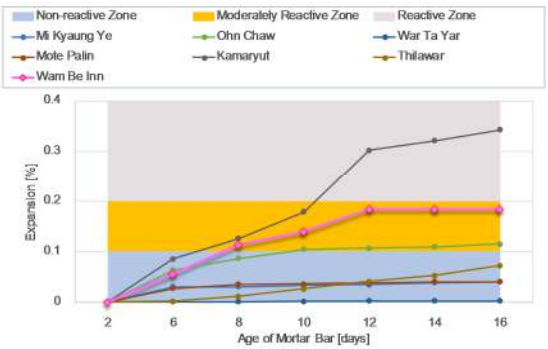

Fig 10 Compared Mortar Bar Expansion and ASR Reactivity Range

3.3 Compared Mortar Bar Expansion and ASR Reactivity Range

It can be clearly seen in Fig.10 that the average expansion rate for Wartayar sand throughout the experiment is very low. So that, fine aggregate from War Ta Yar quarry can be deduced that non-reactive aggregate.

An average expansion of Thilawa sand doesn't reach ASTM's limit of the moderately reactive zone until the end of the experiment. So that, sand from Thilawar sand can be said as non-reactive aggregate.

In Fig 10, the average expansion curve for Kamaryut sand pass through the moderately reactive zone and it reached reactive zone at age of 12 days. Then, expansion rate significantly increases until the end of the experiment: the last test for the age of 16 days. It is clear that sand from Kamaryut

quarry is reactive aggregate.

The average expansion of Wan Be Inn sand at 16 days is 0.184% and that is very close to reach ASTM's reactive zone. It can be said that aggregate from Wan Be Inn quarry is moderately reactive based on the current result.

Average expansion % of MKY-1, 2 and 3 are presented in Fig.10 incorporate with aggregate reactivity classification in accordance with ASTM C-1260. ASTM C-1260 classified that 0 to 1% of expansion of mortar bar of 16 days is non-reactive. So that it can be deduced that river shingle from Mi Kyaung Ye quarry is non-reactive.

The specimen made of aggregate from Ohn Chaw quarry showed the significant increase in expansion from the start to 10 days and those reach 0.1% expansion at the age of 10 days. The average curve of expansion rate stays lower region of the moderately reactive zone in Fig. 5.4. So that, it is concluded that crush aggregate from Ohn Chaw quarry is moderately reactive.

For the mortar bar made up of Moke Pa Lin aggregate, it can be concluded that aggregate form Moke Pa Lin quarry is non-reactive due to the average of expansion for MPL-1, 2 and 3 shown in Fig. 10 stay at the middle of ASTM C-1260 non-reactive zone.

4. Conclusion

In order to identify potential alkali-silica reactivity of fine and coarse aggregate, seven numbers of aggregate quarries located in Myanmar was selected and studied. In the study area, three types of aggregate were observed in which main rock type is naturally found in the study area and the following fact can be concluded.

(a) River shingle from Mi Kyaung Ye quarry is non-reactive aggregate.
(b) Crush aggregate from Ohn Chaw quarry is moderately reactive aggregate.
(c) Fine aggregate from War Ta Yar quarry can be deduced that non-reactive aggregate.
(d) Fine aggregate form Moke Pa Lin quarry is non-reactive aggregate.
(e) Sand from Kamaryut quarry is reactive aggregate.
(f) Sand from Thilawar sand can be said as non-reactive aggregate.
(g) Aggregate from Wan Be Inn quarry is moderately reactive.

References

[1]. M. Berra *et al*., "Alkali-silica reactivity criteria for concrete aggregates," Materials and Structures, vol. 38, no. 3, pp. 373–380, 2005.
[2]. J. A. Farny and B. Kerkhoff, Diagnosis and control of alkali-aggregate reactions in concrete. Skokie, IL: Portland Cement Association, 2007.
[3]. F. Rajabipour *et al*., "Alkali–silica reaction: Current understanding of the reaction mechanisms and the knowledge gaps," Cement and Concrete Research, vol. 76, pp. 130–146, Oct. 2015.
[4]. Z. Owsiak, "Alkali–aggregate reaction in concrete containing high-alkali cement and granite aggregate," Cement and Concrete Research, vol. 34, no. 1, pp. 7–11, Jan. 2004.
[5]. ASTM standard C 1260, 2014, "Standard Test Method for Potential Alkali Reactivity of Aggregates (Mortar-Bar Method)" ASTM International, West Conshohocken, PA, 2014, DOI: 10.1520/C1260-14, www.astm.org.
[6]. U.S.Departemnt of Transportation, Federal Highway Amimistration, M. D. A. Thomas *et al*., Selecting Measures to Prevent Deleterious Alkali -Silica Reaction in Concrete: Rationale for the AASHTO PP65 Prescriptive Approach.

(Received: 8 October 2016, Accepted: 5 January 2017)

Parallel implementation of Entropic lattice Boltzmann method for flow past a circular cylinder at high Reynolds number

Ayurzana Badarch[1,*], KhenmedekhLochin[2], Hosoyamada Tokuzo[3]
[1)]Graduate School of Engineering, Nagaoka University of Technology,
[2)]School of Applied Science, Mongolian University of Science and Technology, Mongolia
[3)]Department of Civil and Environmental Engineering, Nagaoka University of Technology
1603-1 Kamitomioka-machi, Nagaoka 940-2188, Japan
**E-mail: ayur_426@yahoo.com*

Lattice Boltzmann method (LBM) has been receiving enormous attention from researcher to solve fluid related phenomena. LBM in fluid dynamics simulation, one meet some difficulties, for instance it becomes unstable for high Reynolds number flows and requires computational time and memory for large scale simulations. To avoid this, we used here the Entropic LBM (ELBM) of Karlin's group [7] and implemented parallel code on graphical processing units (GPU). For parallel computation, we used GPGPU system of Nagaoka University of technology, which is equipped with Tesla M2050 processors. To verify accuracy and stability, we have solved double periodic shear layer flow in serial computation. The accuracy and stability of simulation by ELBM were superior to the simulation of standard LBM. Simulations of flow past a circular cylinder is carried out by parallel ELBM, where Reynolds number varies up to 140000. Using the GPU in simulation, computation time speeds up until 10 times faster than that of using central processing units (CPU). The results show that the parallel code of ELBM can solve two-dimensional turbulent flow in arbitrary geometry at the higher stability condition without using any other stabilization techniques.

1. Introduction

The simulation of traditional computational fluid dynamics deals with Navier-Stokes equation (NSE). Unlike this, lattice Boltzmann method (LBM) solves the discrete Boltzmann kinetic equation in its simplified form, known as Bhatnagar-Gross-Krook (BGK) equation. Founded in the eighties of last century, LBM become recently a widely used method of computational fluid dynamics (CFD). In LBM, the fluid is simulated by molecular velocity distribution functions with discrete velocities on regular lattice. There are two operations on the distribution functions: streaming and collision. The fluid molecules propagation is described by streaming, which is non-local operation against the local collision operator, describing the collision between molecules [1]. LBM has its intrinsic feature: easy to parallelize on computer [2]. On the other hand, one of long standing problem in fluid flow simulation is the simulation of turbulent flow at high Reynolds number. In CFD, the turbulent flow simulations are usually performed either by computationally expensive direct numerical simulation of NSE or by solving averaged NSE [3, 4, 5, 6]. Direct application of the LBM for the turbulent flow simulation leads to instability of computation, because of the low viscosity of fluid. Laminar flows at low Reynolds number (Re) become turbulent when Re reached the value of Re=300 in the case of flow past a bluff body. One of the promising method of stabilizing the LBM turbulent computation is the entropic LBM (ELBM) of Karlin's group, in which, the distribution functions are straightened to satisfy the maximum condition of the entropy at the every time step of simulation. In this paper, first we confirm accuracy and performance of the ELBM solving double periodic shear layer flow. Then we perform the calculations of high Reynolds number turbulent flow past a circular cylinder using the ELBM of Karlin et al [7, 8] in parallel algorithm.

2. Numerical model

Recently, a simple entropic stabilizer was proposed to stabilize LBM simulation at high Reynolds number in incompressible flow. The entropy of the lattice Boltzmann equation (LBE) can be written as

$$S[f] = -\sum_{i=0}^{8} f_i \, ln\left(\frac{f_i}{w_i}\right), \tag{1}$$

where f_i is the density distribution functions, w_i is the weight and $S[f]$ is the entropy. Further we write the f_i as a component of the velocity moments:

$$f_i = k_i + s_i + h_i, \tag{2}$$

where k_i is the kinematic part of populations, which depends only on the locally conserved fields, s_i is the shear part of populations, which depends on the stress tensor and h_i is the higher order moments of populations as a linear combination of the remaining higher order moments. Introducing deviations $\Delta s_i = s_i - s_i^{eq}$ and $\Delta h_i = h_i - h_i^{eq}$, the extremum condition of the $S[f]$ take the form:

$$\sum_{i=0}^{8} \Delta h_i \ln\left(1 + \frac{(1-\beta\gamma)\Delta h_i - (2\beta-1)\Delta s_i}{f_i^{eq}}\right) = 0, \tag{3}$$

where β can be defined from the kinematic viscosity as $\nu = c_s^2\left(\frac{1}{2\beta} - \frac{1}{2}\right)$ and the maximum of stabilizer γ can be computed as

$$\gamma^* = \frac{1}{\beta} - \left(2 - \frac{1}{\beta}\right)\frac{\langle \Delta s | \Delta h \rangle}{\langle \Delta h | \Delta h \rangle} \text{ with } \langle X|Y \rangle = \sum_{i=0}^{8} \frac{X_i Y_i}{f_i^{eq}}. \tag{4}$$

Non equilibrium part of the distribution function can be written as

$$f_i - f_i^{eq} = \Delta s_i + \Delta h_i, \tag{5}$$

and it is used for calculation of higher order moments Δh_i. The deviations of shear part of the populations are defined by following velocity moments:

$$\begin{cases} \Delta s_0 = \rho\left(4uv\widetilde{\Pi}_{xy} - \left[\dfrac{u^2 - v^2}{2}\right]\widetilde{N}\right), \\ \Delta s_{1,3} = \dfrac{\rho}{2}\left(\left[\dfrac{1 + cx_i u + u^2 - v^2}{2}\right]\widetilde{N} - [2cx_i v + 4uv]\widetilde{\Pi}_{xy}\right), \\ \Delta s_{2,4} = \dfrac{\rho}{2}\left(\left[\dfrac{-1 - cy_i v + u^2 - v^2}{2}\right]\widetilde{N} - [2cy_i u + 4uv]\widetilde{\Pi}_{xy}\right), \text{ and} \\ \Delta s_{5,6,7,8} = \dfrac{\rho}{4}\left([4uv + cx_i cy_i + 2cy_i u]\widetilde{\Pi}_{xy} + \left[\dfrac{-u^2 + v^2 - cx_i u + cy_i v}{2}\right]\widetilde{N}\right), \end{cases} \tag{6}$$

where $\widetilde{\Pi}_{xy}$ and $\widetilde{N}$ are the central moments and cx_i and cy_i are the discrete velocities of lattice. The central moments are defined by the natural moments and velocities as

$$\widetilde{\Pi}_{x,y} = \sum_{i=0}^{8} f_i cx_i cy_i - uv \text{ and } \widetilde{N} = \sum_{i=0}^{8} f_i cx_i^2 - \sum_{i=0}^{8} f_i cy_i^2 - (u^2 - v^2). \tag{7}$$

After defining stabilizer with above formulas, the post collision state of distribution function is computed in the form:

$$f_i' = f_i - \beta(2\Delta s_i + \gamma^* \Delta h_i) \tag{8}$$

and the streaming is done by copying distribution functions to their designated directions. The equilibrium distribution functions are defined by the Maxwell distribution as

$$f_i^{eq} = w_i \rho\left[1 + \frac{\mathbf{c}_i \cdot \mathbf{u}}{c_s^2} + \frac{(\mathbf{c}_i \cdot \mathbf{u})^2}{2c_s^4} - \frac{\mathbf{u} \cdot \mathbf{u}}{2c_s^2}\right], \tag{9}$$

where ρ is the density, $\mathbf{c}_i$ is the discrete velocity and $\mathbf{u}$ is the macroscopic velocity. The density and velocity are estimated by the moments of the distribution functions as

$$\rho = \sum_{i=0}^{N} f_i, \quad \rho \boldsymbol{u} = \sum_{i=0}^{N} \boldsymbol{c}_i f_i. \tag{10}$$

The collision expression given in Eq. 8 is called KBC operator in Entropic LBM [7], while standard LBM uses BGK operator for collision.

3. Parallel implementation of the Entropic LBM

In this study, standard and entropic LBM are implemented in serial and parallel way using Fortran 90 programming language. A stable computation of the ELBM is gained by paying time and memory as the computational cost, which will be explained in the Section 5. At the other points, engineering problems are often characterized as a large scale or long term phenomena in space and time. LBM solution for these problems in CPU based simulation ended up at difficult challenges because of the computational cost. The implementation of the ELBM on GPU can solve the two important difficulties of computation: instability and high computational cost.

Nagaoka University of Technology (NUT) has a GPGPU system, which is available for students and staffs for their research activities. The GPGPU system is powered by 16 nVIDIA Tesla M2050 graphic processing units, which has ability to perform 562GFLOPs in double precision. Also CUDA Fortran version 11.3 has been installed on the GPGPU system. Grasping this technical potential and numerical method, we have made an attempt to implement efficient parallel code for fluid flow on GPU. In CUDA programming, code has to be devoted to two particular sections named host code and device code [9], as shown in Fig. 1. Host code refers that code executes on the host CPU machine, whereas device code refers that code executes in the GPU machine. The codes use memories on dedicated machines, i.e., variables used in device code must use a GPU memory.

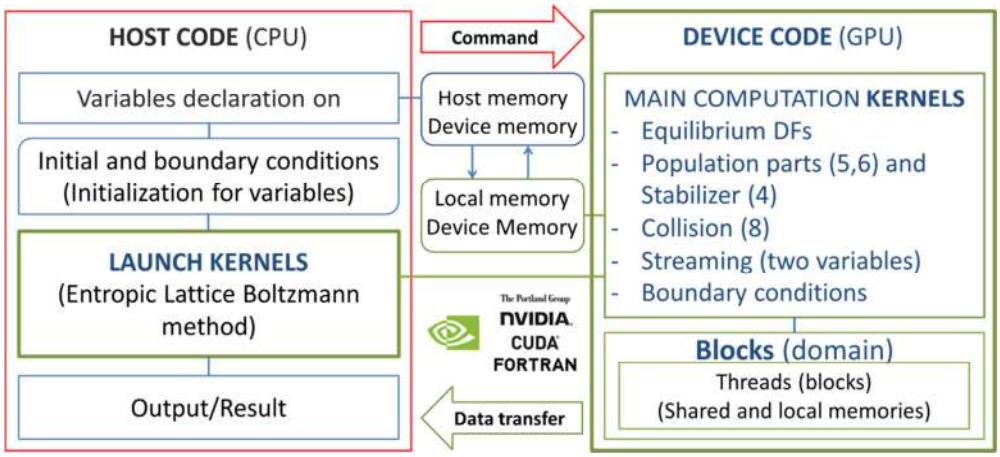

Fig. 1 General architectural scheme of the implemented parallel code on the GPGPU system.

As the main program in the CUDA FORTRAN code is executed on the host, all variables in both host and device codes need to be declared specific memories of their use in the host code. Macroscopic variables, distribution functions and population parts are declared on the global memory (device memory) and could only be used in device code. As purpose of the ELBM code, initial condition and loading geometric data are implemented on the host code, in which device and host codes need to exchange data. So called kernels, subroutines of Fortran language, implemented for device code is launched from the host code. On the right hand side of Fig. 1, the host code composing the kernels with used equations is given, which is performed on the predetermined blocks and threads in GPU architecture. An entropic part of the numerical algorithm tested as separated kernels, for instance a kernel for population part and a kernel for stabilizer. The separated kernels use low memory consumption, however, total computation time of two kernels were higher than their unified version in one kernel. The defining population parts and stabilizer is optimized to use low memory on the local memory of the GPU in one kernel, since the declaration of array in the kernel use a lot of registration, which might be caused the abortion of the kernels. Besides the streaming step, all required equations and formulas in the ELBM are easily implemented in parallel way. To perform the streaming in efficient way, two parallel distribution functions are used and they

synchronize in the host code after the calculation of one time step. To improve performance of parallel code, some optimization of array declaration as $f(x,y,i)$ for distribution function instead of the regular array structure of distribution function $f(i,x,y)$ is applied. Storing the constant parameters used in both code in their memory save small amount of the computational time. A single lattice is assumed to be a thread and a computational domain has divided as blocks horizontally.

4. Numerical test on doubly periodic shear flow

Doubly periodic shear layer flow is often considered a benchmark [7,10] case for under-resolved simulation of smooth flows with sharp features. Shear flow had been solved by serial code of standard LBM and ELBM in resolutions of N=128, 256, 512, and 1024. Initial conditions for flow field are given by

$$\begin{cases} u = \begin{cases} u_0 tanh\left(k\left(\frac{y}{N} - 0.25\right)\right), y \le N/2, \\ u_0 tanh\left(k\left(0.75 - \frac{y}{N}\right)\right), y > N/2, \end{cases} \\ v = \delta u_0 \sin\left(2\pi\left(\frac{x}{N} + 0.25\right)\right), \end{cases} \tag{11}$$

where $k(=80)$ is the parameter controlling the width of the shear layer and $\delta(=0.05)$ is the parameter creating small perturbation of velocity in y-direction, which initiates a Kelvin-Helmholtz instability. The turning over time of the shear layer is defined as $t_c = N/u_0$, where $u_0(=0.04)$ is the initial velocity defining Reynolds number for flow as $Re = u_0 N/\nu$. In numerical test, Reynolds number was set at 30000. The simulation results of vorticity at t_c by two methods are shown in Fig. 2 in order of grid resolutions. The simulation of standard LBM was failed before the convergence of the under-resolution at low resolution of domain, for instance unstable appears at t = 2200 before the vortex roll-ups in the interface of shear layers, shown in top figure of Fig. 2 (a).

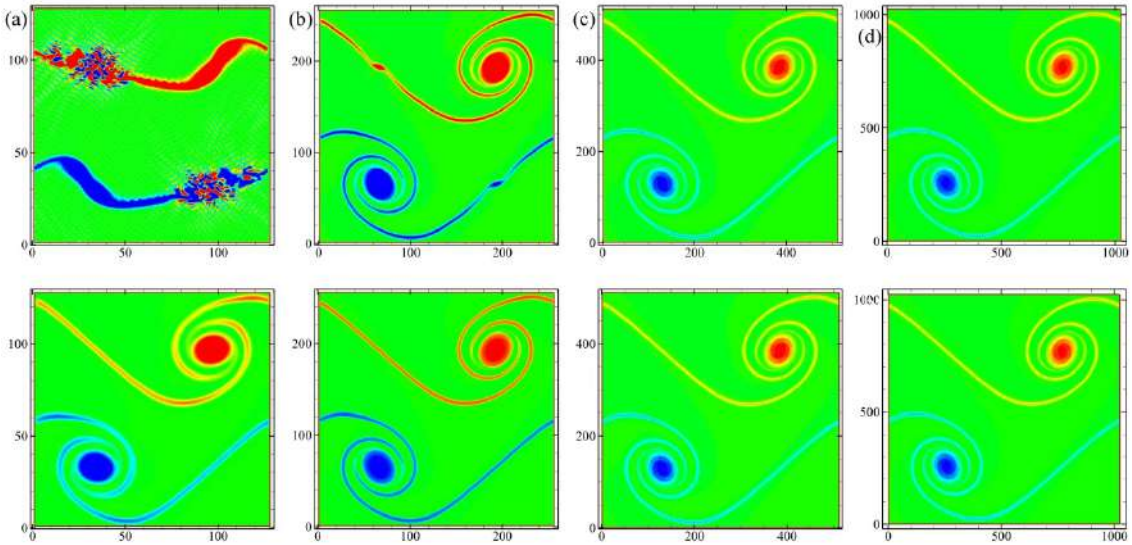

Fig. 2 Double peroidic shear layer flow simulations on the different grid resolutions. Top figures were produced by using the standard LBM, while bottom figures were produced by using the entropic LBM. Vortex roll-ups appears at (a) t_c=3200, (b) t_c=6400, (c) t_c=12800 and (d) t_c=25600.

As an increase of grid resolution, relaxation time of the standard LBM increases and the computation become rather stable. The computation successfully survived on the further cases of simulations in the case of standard LBM. However, as shown in top of Fig. 2 (b), two small additional roll-ups created at linear part of vortex field, which is the source of unstable solutions. As expected shapes of vortex, entropic LBM produces flow field at the even small resolution of grids and additional

roll-ups emerging from unstable of the numerical solution does not appear in any case of simulation. This stable simulation can be performed at very small kinematic viscosity due to the coarse grid and high Reynolds number. The stabilizer in ELBM is a self adaptive local parameter and impacts on the resolving of the flow fields. The distribution of the stabilizer and its value range do not depends on the Reynolds number. For computational cost of the serial codes, ELBM code was 2 to 4 times slower than the standard LBM code.

5. Parallel performance of the ELBM code

The parallel code for ELBM is implemented by the way that uses lower memory and efficient computation, as explained in the Section 3. We have solved flow past a cylinder in laminar regime (Re = 200) to evaluate performance of the parallel code, since the standard LBM can't survive at high Reynolds number. The simulation domain formed as 300 grids in length and 100 grids in width. The simple bounce back boundary condition was imposed for top wall, bottom wall and a circular obstacle. The Zou/He boundary condition was applied with a characteristic velocity of u_0=0.1 for inlet and the zero gradient boundary condition is used for outlet boundary. PGI Fortran compiler on the GPGPU system is used to perform parallel and serial computations to evaluate parallel performances. Time criteria to stop simulations was set at t = 50000 in all simulations.

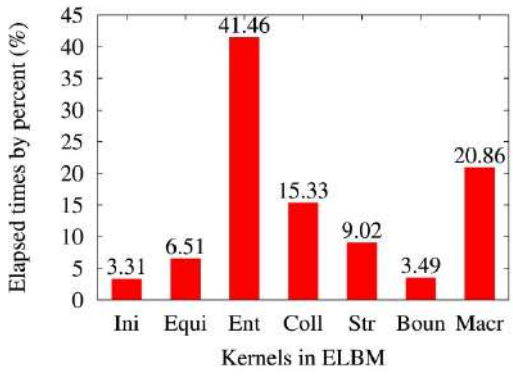

Fig. 3 Percent of elapsed times used by the kernels in single computational time of the ELBM in double precision.

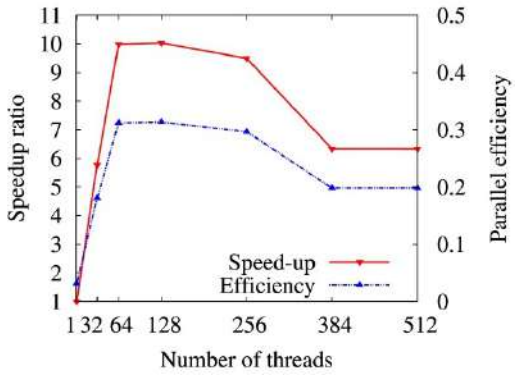

Fig. 4 Speedup ratio and parallel efficiency of the ELBM code with regards to the number of threads.

As investigating deeply the performance of the parallel ELBM code, Entropic part (labeled "Ent" in Fig. 3), computing stabilizer and population parts, consumes around 41% of the all required time to perform kernels, shown in Fig. 3. The second largest consumer was defining macroscopic variables and synchronization of two groups of distribution functions (labeled "Macr" in Fig. 3), since the streaming process done by using the two groups of distribution functions.

The computational domain was divided as blocks in horizontally and threads in a block. A number of blocks can be chosen. Figure 4 shows speedup ratio and parallel efficiency of parallel computation on GPGPU with respect to the number of threads used in simulation. The parallel efficiency is determined as the ratio between the speedup ratios to the warp sizes of GPU. The parallel code can speed up until 10 times faster than its serial version on the same machine. The highest speedup ratio was found at the 64 threads in a block. The computational efficiency would be convenient where the number of threads is lower than the maximum grid number of domain. In the other words, the number of threads should be smaller than the maximum number of grid in horizontal or vertical direction.

Further we examined computational throughput and memory bandwidth for four cases of grid resolutions, shown in Fig. 5. The number of thread was 512 in the simulations. Computational throughput and memory bandwidth have linear relation with the grid resolutions. Comparing to the maximum performance of the GPU, our code performs at the middle rate. Actually, memory band width was inefficient, uses small amount of the possible memory bandwidth for the data transfer and

management. Therefore, effective usage of the memory band width for parallel ELBM code needs to be improved. Elapsed time against the increase of grid resolutions plotted in Fig. 6 shows performances of the code on the different grid resolutions. Hence, the increase of the computational time has parabolic relation with the increases of grid resolution. Steepness of the parabola can be decrease if we increase effective memory bandwidth in the code. To improve effectiveness of the code, possible kernels can be merged in such a way that uses low memory in local memory of the device. Interestingly, LBM index, which is index to show parallel performance of the LBM in the way that how much lattice is updated per second (LUPs), increased as the grid resolution increases in Fig. 6.

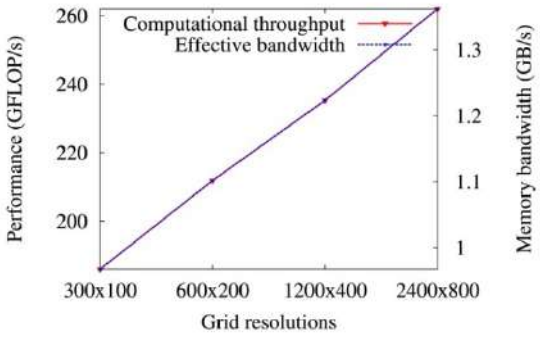

Fig. 5 Computational throughput and memory bandwidth against the grid resolutions

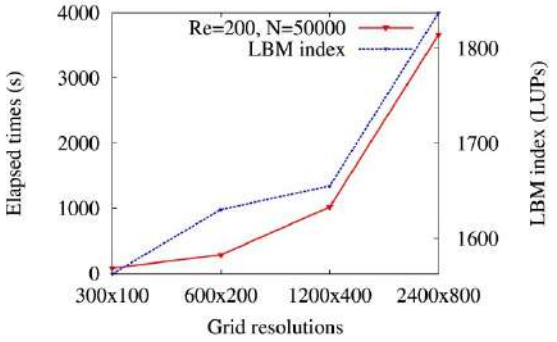

Fig. 6 The elapsed time and efficiency of ELBM computation against the grid resolutions

6. Numerical simulation of flow past a cylinder

Flow past a bluff body has been widely studied both numerically and experimentally [13] at high Reynolds number [3-6]. The enhanced version of LBM using sub-grid scale [11, 12] and direct numerical simulation like entropic approaches [7, 8] are the main contributions for those studies. We have used a domain used in [12] for our simulation. The boundary conditions are the same explained in section 5. Preliminary test simulations were performed for the Re=1000 and Re=3900 in order to test accuracy. We defined Strouhal number and compared with the other studies conducted in same condition using different techniques in Table 1.

Table 1 Strouhal numbers of flow around circular cylinder at different Reynolds number

Sources/methods of the results	Strouhal number
Re = 1000 – Present study	0.217
Extended LBM (using Smagorinsky sub-grid scale model) [12]	0.208
Experiment [13]	0.212
Standard k-epsilon model [5]	0.148
Re = 3900 – Present study	0.211
Extended LBM (using Smagorinsky sub-grid scale model) [12]	0.215
Experiment [13]	0.215
Standard k-epsilon model [5]	0.171
Re = 140000 – Present study	0.228
Extended LBM (using Smagorinsky sub-grid scale model) [12]	0.209

The Strouhal numbers defined by ELBM was in good agreement with the results of experiment

and other simulation methods. In Fig.7, the vorticity field of fully developed 2D turbulent flow at simulation time t = 10000 at Re = 140000 performed by parallel ELBM is visualized.

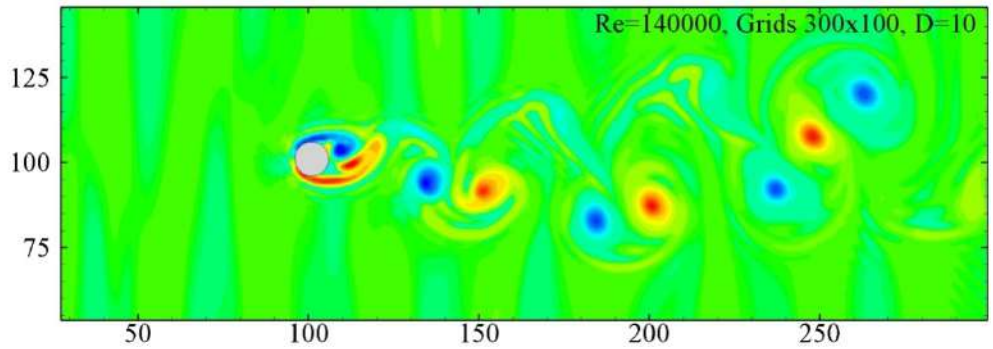

Fig. 7 Vorticity field of flow past cylinder at Re=140000 on coarse grid.

A performance of the ELBM can clearly describe Reynolds number effect on the cylinder. The flow field can be captured exactly comparing with performance of LBM extended by Smagorinsky model. It was revealed that Smagorinsky model for LBM overestimates eddy viscosity [14] at high Reynolds number and it leads underestimates of velocity field. Unlike it, ELBM does not modify viscosity in the simulation and corrects velocity field by the maximum entropic condition. For coarse grid, ELBM can resolve flow field and generate vortex in sub-grid. Figure 8 shows the pressure coefficient distribution and the velocity magnitude in lattice form around the cylinder defined at Re = 140000. Based on the results obtained by ELBM, flow field can be computed with reasonable accuracy and stability at very high Reynolds number using ELBM. It should be noted that the bounce back boundary condition might be affected on the accuracy in some case [7]. In that case, proper boundary condition based on kinetic theory must be used [15].

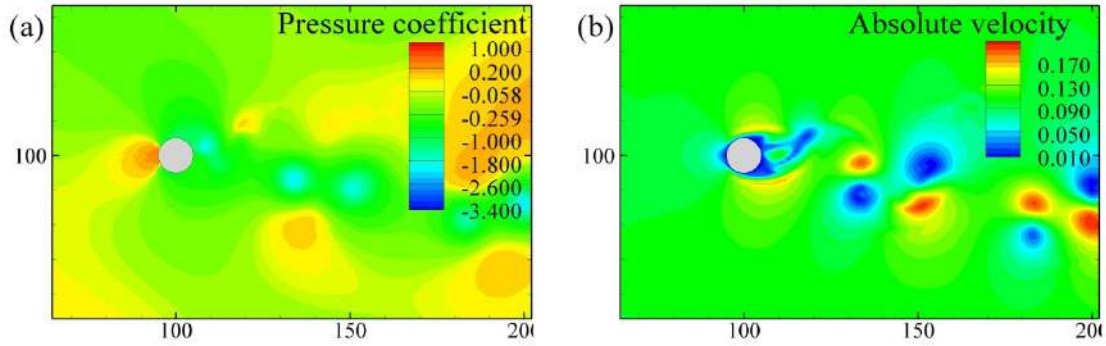

Fig. 8 Pressure coefficient distribution and absolute velocity value at Re=140000

7. Conclusion

We have implemented Entropic Lattice Boltzmann method in parallel operation using CUDA Fortran programming language on the NUT's GPGPU system. Entropic LBM is used to perform unconditionally stable simulation, while parallel computation is used to speed up simulations and improve efficiency of code for the future large scale engineering simulations. The parallel code is aimed to be used for large scale and long term simulation in engineering field in complicated geometry at high Reynolds number fluid flow. Numerical accuracy has been tested on doubly periodic shear layer flow and compared with the solution of the standard LBM. Further, we solved flow past a cylinder at Re=140000 to show performance of the ELBM parallel code. To evaluate accuracy, Strouhal number at Re=1000, 3900 are defined and compared with experiment and other numerical simulation results. The results were in good agreement. The parallel code of the ELBM is

implemented in the combination of low memory usage and fast computation. Using GPGPU for ELBM, the computation can be performed 10 times faster than serial code. Based on the stable and accurate computation of ELBM, parallel computation will be very efficient method for CFD.

Acknowledgments

Authors would like to express their gratitude to Prof. Tomohiro Degawa for whose valuable advices and comments during the implementation and improvement stages of the parallel code.

References

[1] Succi S. The lattice Boltzmann equation: for fluid dynamics and beyond. Oxford university press, 2001.

[2] Bailey, Peter, et al. "Accelerating lattice Boltzmann fluid flow simulations using graphics processors." 2009 International Conference on Parallel Processing.IEEE, 2009.

[3] Mittal, R., and S. Balachandar. "Effect of three□dimensionality on the lift and drag of nominally two□dimensional cylinders." Physics of Fluids, Vol.7.8, pp. 1841-1865.1995

[4] Karabelas, S. J. "Large eddy simulation of high-Reynolds number flow past a rotating cylinder." International journal of heat and fluid flow, Vol. 31.4, pp. 518-527.2010.

[5] Rahman, MdMahbubar, MdMashud Karim, and Md Abdul Alim. "Numerical investigation of unsteady flow past a circular cylinder using 2-D finite volume method." Journal of Naval Architecture and Marine Engineering, Vol.4.1, pp. 27-42.2007.

[6] Rajani, B. N., A. Kandasamy, and SekharMajumdar. "LES of Flow past Circular Cylinder at Re= 3900." Journal of Applied Fluid Mechanics, Vol.9.3, 2016.

[7] Karlin, I. V., F. Bösch, and S. S. Chikatamarla. "Gibbs' principle for the lattice-kinetic theory of fluid dynamics." Physical Review E, Vol.90.3, pp. 031302.2014.

[8] Ansumali, Santosh, et al. "Entropic lattice Boltzmann simulation of the flow past square cylinder." International Journal of Modern Physics C, Vol.15.03, pp. 435-445. 2004.

[9] Ruetsch, G. and Massimiliano, F. "CUDA Fortran for scientists and engineers." NVIDIA Corporation, 2701. 2011.

[10] Brown, David L. "Performance of under-resolved two-dimensional incompressible flow simulations." Journal of Computational Physics, Vol 122.1, pp. 165-183.1995.

[11] Hou, Shuling, et al. "A lattice Boltzmann subgrid model for high Reynolds number flows." arXiv preprint comp-gas/9401004. 1994.

[12] Liu, Tiancheng, et al. "Extended lattice Boltzmann equation for simulation of flows around bluff bodies in high Reynolds number." International Colloquim on Bluff Bodies Aerodynamics, pp. 1-16. 2008.

[13] L. Ong, J. Wallace. The velocity field of the turbulent very near wake of a circular cylinder, *Exp. Fluids, Vol* 20, pp. 441, 1996.

[14] Ayurzana, B. "Free surface flow through porous media by Lattice Boltzmann method."Proceedings of the Mongolian Academy of Sciences, vol 56.01, pp. 42-54. 2016.

[15] Chikatamarla, S.S. and Karlin, I.V. "Entropic lattice Boltzmann method for turbulent flow simulations: Boundary conditions." Physica A: Statistical Mechanics and its Applications, 392(9), pp.1925-1930 , 2013

(Received: 7 October 2016, Accepted: 11 January 2017)

A Study on the Relationship between the Mindset of Taxi Drivers and the Attribution of Accident Causes and Driving Behavior

Makiko Okamoto[1], Katsuko Nakahira,T[2,*]
[1)]Department of System Safety, Nagaoka University of Technology,
[2)]Department of Information and Management System Engineering, Nagaoka University of Technology,
1603-1 Kamitomioka-machi, Nagaoka 940-2188, Japan
**E-mail: okamoto@kjs.nagaokaut.ac.jp*

In the field of Education, a learner's mindset(the incremental mindset [abilities can be developed through effort] and the entity mindset [abilities are static and unchangeable]) is thought to influence one's learning motivation. The prior enables learning motivation to be maintained even after failures because the failure is attributed to a lack of effort, and the issue can thus be resolved with more effort. It has been shown that drivers who attribute their accidents to a lack of effort, experience fewer accidents. The purpose of this study was to reveal the relationship between the mindset of drivers and attribution of accident cause, driving behavior. Results showed that there were positive correlations between incremental mindset and the causal attribution of "everyday effort", higher accident rate and longer driving distance. The group with incremental mindset(ITG) was more likely to have accident models that involved other persons. The study showed the possibility that ITG had higher accident rates since they considered themselves to be able to "generate higher revenue," rather than "prevent accidents" with effort, and engaged in long-distance driving that could lead to accidents. The results may be utilized in basic materials that can be provided to drivers for precise safety education.

1. Introduction

It has been indicated that, in traffic safety education, it is desirable to teach accident prevention in which the individual is the main factor in causing the accident, without attributing it to outside factors such as others of traffic [1]. Using a questionnaire, Yamashita[2] found that, in a situation in which the occurrence of an accident is assumed, individuals who have an attitude of strictly taking responsibility on themselves have a more desirable attitude toward safety, including egocentricity and impulsivity, when compared to individuals who pass the responsibility onto others. Further, a questionnaire survey revealed that the none accident group demonstrated higher attribution of the cause of the accident to themselves when compared to the accident-prone group. Yamashita[2] attempted to explain this as a causal attribution for "failure." In the event of a failure, i.e., meeting with an accident, the accident-prone group attributed it, not to themselves, but to the external situation or a mistake of the other party. In contrast, the low-accidents group attributed it to their own lack of driving ability or lack of effort in confirmation, and as such, they have an increased motivation to try to improve themselves, which makes them more safe drivers. Therefore, an attitude of attributing responsibility to oneself is considered important in accident prevention.

On the other hand, the aforementioned research did not reveal which attribution to effort or ability was important among the self-related factors. In this regard, it is meaningless whether it is effort or ability, because, while the feeling that one is able to control the target of attribution is important, it has been pointed out that a distinction between the two is meaningless [3].

However, in terms of education, regarding the difference between causal attribution to effort/ability, it is known that the student's own ability combined with their perception of intelligence (mindset), governs the pattern of behaviors and emotions that occur, mainly in the

context of academic achievement. In this context, we need to consider the incremental theory and entity theory. The former is the idea that one's ability changes, and if one puts forth effort, abilities can improve. The incremental theory group (ITG), which focuses on the improvement of one's own ability and is aimed at the acquisition of knowledge (Mastery goal), attributes the cause of facing difficulties and failings to personal lack of effort, is motivated by resolution using strategies different from those of the past, and is less likely to experience negative feelings. On the other hand, the entity theory is the idea that ability is innate and that it is difficult to control it. Therefore, the entity theory group (ETG), which focuses on avoiding low assessments of one's own abilities (performance goal), attributes the cause of failure to personal lack of ability, and, as its adherents are of the position that failure has exposed their own low capacity to those around them, negative feelings are likely to occur, their motivation for subsequent challenges is reduced, and they become evasive [4]. Thus, in the context of learning, the incremental theory is tied to an attitude of active participation in the classroom and is generally considered more effective in the promotion of learning as compared to the entity theory of intelligence [5]. Additionally, in the industrial sector, employees who focus on the learning objective related to the incremental theory show a positive correlation between effort and business performance, which is mediated by self-regulation relating to setting goals, effort, and planning [6]. Therefore, a correlation between mindset and academic/business performance is evident to some degree.

On the other hand, in the case of driving businesses like buses and taxis, not only improvement of business performance, but preserving the safety of passengers and other people in traffic is also important. However, the relationship between mindset and accidents that may occur accompanying this business is not clear. Accordingly, the aim of this study was to reveal the relationship between the driver's mindset and his/her causal attributions of accidents, as well as the driving behavior and accidents observed in professional drivers. The aim was to extract points for developing an effective educational intervention.

The study was conducted with the ethics approval of Nagaoka University of Technology.

Survey 1

2-1 Experimental method

(1) Mindset assessment scale (explicit mindset)

A questionnaire was designed based on a scale created by Hong et al. [7]. This questionnaire contained 3 questions, and used six-point scale. In our survey, a higher response score indicates a tendency to subscribe to the incremental theory. Note that, in order to clarify that "ability" pertained to driving, "ability to drive a car" was used rather than "talent." As this questionnaire attempted to measure the mindset that the experiment participants themselves were explicitly aware of, it was referred to as the explicit mindset.

(2) Causal attribution scale

With reference to the work of Nasu et.al.[8], a self-assessment with the scene imagination method was used. Specifically, subjects were asked to envision a scene in which they encountered an accident while they were driving. The attributed cause of the accident had six classifications, the efforts just before (the efforts just before the accident directed towards avoiding it), normal effort (efforts directed at driving safely in normal circumstances), ability, physical condition, luck, and other traffic. Each item had two questions, with a total of twelve questions. Responses were made on a six-point scale. A higher value for a response demonstrates a higher amount of attribution to that factor.

(3) Mindset IAT (implicit mindset)

Mindset was measured using a self-report questionnaire that is used to assess an explicit mindset obtained as a result of the individual's introspection. However, as responses may be biased towards social desirability and are influenced by personal introspection, it has been indicated that it may be difficult to measure genuine mindset using this method. Accordingly, in addition to the questionnaire, an implicit attitudes measure, known as the Implicit Association Test (IAT) [9], was used in the present study. The IAT is a method of measuring the strength of ties between concepts from the

response time taken while sorting words into specific categories in a vocabulary grouping task. It has been demonstrated that unconscious behaviors conventionally considered difficult to measure can be measured to some degree by using this technique [10]. In the present study as well, we attempted to observe correlations relating to accidents that could not be measured using an explicit indicator like a questionnaire.

IAT categories and stimulus words were created based on the work of Fujii et.al. [11]. Subjects classified stimulus words associated with the attribution categories of “changes” and “does not change,” and the two types of attribution categories of “intelligence” and “luck” in seven reaction blocks into the presented categories, as fast as possible, using a key on a notebook PC. Note that, though the stimulus words were fundamentally derived from those used by Fujii at.al[11], as the present survey target was driving-related ability, “scholarly ability” was replaced with “driving ability.” Scoring was conducted according to the technique suggested by Greenwald et al. [12]. A higher score indicated a higher implicit tendency for subscribing to the incremental theory.

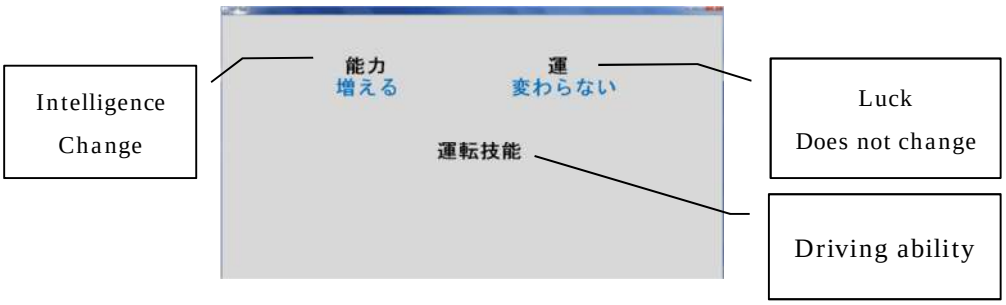

Figure 1 Example of IAT screen used in this survey

2-2 Experiment participants

Participants were thirty-eight taxi drivers (all male, average age 57.34 years, *SD*=11.84 years) .

2-3 Procedure

The participants were led to an experiment hall prepared by the subcontracting company in advance, and the details of the experiment were explained. It was conveyed that the experiment results would be statistically analyzed, individual data would not be publicly announced externally—including to the subcontracting company—in a format that could be identified, the experiment results would not be related to professional assessment of the experiment participant, and the experiment could be stopped midway if requested. Subsequently, after explaining the mindset IAT implementation method while demonstrating it on the screen of the notebook PC, the experiment was carried out, and when completed, the experimenter informed the participant accordingly. Next, a questionnaire with the mindset assessment scale and the causal attribution scale was presented in random order. After completing the questionnaire, the structure of the mindset IAT and the research objectives were explained to the participant. Further, in order to confirm the test-retest reliability of the mindset IAT, it was carried out a second time either one week or ten days after the initial assessment. None of the participants reported that they wished to stop the experiment midway.

2-4 Accident rate and mindset

We examined the relationship between the number of accidents occurring between December 16, 2009 and April 30, 2014, and mindset. Note that, as the period of membership with the subcontracting company differed across participants, the number of accidents was divided by the investigation period to calculate the accident rate during the investigation period. For participants who began membership with the subcontractor after the investigation period had begun, the number of accidents was divided by the actual membership period.

2-5 Result

A positive correlation was observed between explicit mindset and normal effort (r=0.34, p<0.05). A significant correlation between implicit mindset and causal attribution was not observed.

A significant correlation between explicit mindset and implicit mindset was not observed.

A relatively strong correlation was observed between the first and second mindset IAT results

Table1 Correlations of mindset, attribution of cause, accident rate

	Explicit MS	Implicit MS	Efforts Just Before	Normal Effort	Normal Others	Others Just Before	Mood, PC	Luck	Ability	Accident rate
Explicit MS	1	0.2	-0.14	0.34*	-0.22	-0.19	-0.09	-0.21	0.11	0.50**
Implicit MS		1	0.06	0.21	0.09	-0.1	-0.03	0.11	0.16	0.12

(r=0.48, p<0.05).

A positive correlation was observed between explicit mindset and accident rate (r=0.50, p<0.05), whereas a significant correlation was not observed for implicit mindset(Table 1).

3.Survey 2

3-1 Distance traveled and mindset

The correlation between 7 months in 2014 distance traveled and mindset was investigated. Note that, as this was an actual behavioral observation rather than a laboratory experiment; therefore, the significance level was set to 10%. Additionally, in order to control for the effect of the number of workdays, the average distance traveled for one workday (the total kilometers traveled during the investigation period divided by the total word days) was used.

As a result, a weak positive correlation was observed between explicit mindset and average distance traveled; a trend was observed in which the higher the mindset, the longer was the average distance traveled (r=.28 p=.09). A significant correlation with implicit mindset was not observed.

3-2 Accident type and mindset

The experimenter extracted the participants' behavior type at the time of an accident from the accident circumstances and the sketch of the scene described in the accident reports collected by the subcontracting company for the accidents that were included in the analysis for section 2-4, and compared the findings between the incremental and entity groups. With regard to these groups, using the average response on explicit mindset as a standard, those with a high average value were placed in the incremental group and those with a low value were placed in the entity group. As a result, when the incremental group was compared to the entity group, they had more accidents during course changes, left and right turns, and departure. Meanwhile, the entity group had more single-accidents while backing up and going straight (Table 2).

Table 2 Result of accident type and mindset

Behavior Type Group	Course changes	Left right turns	Departure	Backing up	Going straight	Parking/stopping	Opening/closing doors	Total
ITG	12	9	8	0	4	11	3	47
ETG	5	2	4	9	9	11	2	42

3-3 Accident report form entries and mindset

The accident circumstances were entered in the accident report form used in 3-1, by the driver who was involved in the accident. This included the facts and causes of the accident. Consequently, the cause of the accident was described based on their subjective judgment. Accordingly, from the description of the accident circumstances, the experimenter classified the participants based on whether the cause of the accident was attributed to themselves or the other party. For example, if the

participant used "...hit," it would be attributed to themselves, and he used "...was hit by," it would be attributed to the other party. Accidents in which the causal attribution could not be understood by reading the description were omitted.

Using this data, when a chi-square test was conducted to compare the incremental and entity groups in terms of their attributions of the cause of the accident, the incremental group was found to attribute the cause to the other party more frequently (χ^2=4.62, df=1, p<0.05)(Table 3).

Table 3 Result of causal attribution that was read from the description of the accident reports and mindset

	Group	ETG	ITG	Total
Causal Attribution	The Other Party	16	28	44
	Themselves	25	17	42
Total		41	45	86

4. Discussion

The results are summarized in Figure 2.

When those with ITG were asked to imagine a scene of encountering an accident and respond, they generally attributed the cause of the accident to their own effort. However, when they specifically described the circumstances of an accident they had actually encountered, they exhibited a tendency to consider the other party to be the cause. Additionally, in terms of behavior type, the ITG had more accidents in settings where their own vehicle was accompanied with changes in traveling direction, like when changing course, turning left or right, or departing. In particular, when looking closely at the details of the descriptions of the circumstances in which the accidents occurred, we observed more cases in which the course of the vehicle had changed according to the directions of a passenger or when the driver found a passenger. Further, an overall tendency to travel for longer distances for business was observed in the ITG.

As evident from the good performance of the employees with a strong learning goal focus that is linked to the incremental theory, the concept that "ability can increase with effort" is thought to be specifically represented in the idea that "if one puts forth effort, one's performance improves." Considering that if one puts forth effort one's business the revenue would increase, it is possible that driver believe that lengthening the distance traveled, actively looking for passengers, as well as trying to drive in response to the passenger's wishes would help increase income.

Further, the tendency of ITG participants to attribute the cause to their own lack of effort when imagining a general accident encounter, but to attribute the cause to other parties when they

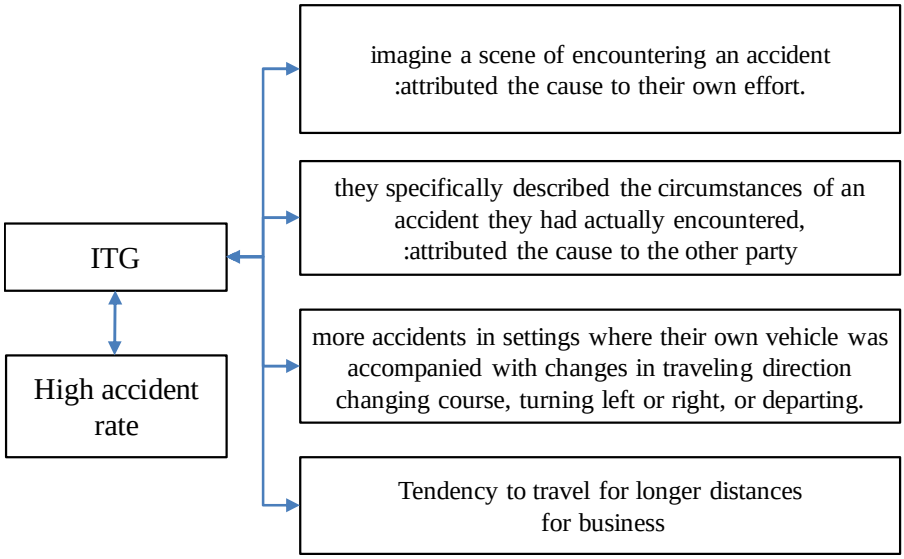

Figure 2 Summary of results

themselves are faced with an accident seems contradictory. However, taxi drivers have the opportunity to receive traffic safety education through lectures, etc. within their companies. At such events, they are taught that their "efforts in preventing accidents are indispensable," and as a result, it is possible that they answered with the common belief that one's own lack of effort is the cause of an accident. Meanwhile, regarding cases in which they actually encounter an accident, the effect of a self-justification bias according to the cognitive dissonance theory needs to be considered [13]. Specifically, it is possible that when one encounters an accident while "one is putting forth effort" to improve business revenue, he/she thinks "I, who was putting forth effort, caused an accident to occur," which leads to cognitive dissonance. Therefore, one may describe the other party as the cause to strike a balance.

Finally, we did not find a relationship between implicit mindset and driving behavior, etc., because all of the items surveyed were conscious behaviors, while the IAT used in this study measured unconscious behavior [10]. As the descriptions on the accident report forms were filled in based on the driver's own explicit consciousness, i.e., distance was used as an indicator of performance, and the driving behavior shown, such as turning left or right, was used as behavior type at the time of the accident, all of which are consciously conducted behaviors, it is thought that they were not subjects for the IAT prediction.

5.Conclusion

The above findings indicate that the stronger the incremental tendency in the mindset of the driver, the more they think, "if I put forth effort, my performance will increase," and consequently, their distance traveled increases, and their tendency to attach importance to the passenger becomes stronger. This may also lead to focusing too much on the presence of a passenger and not sufficiently checking one's surroundings, or driving continuously without breaks to increase performance. Accordingly, with respect to the relationship between effort and performance, as an educational intervention for this group of drivers, it is necessary to focus on helping drivers to be aware of their own cognition, as well as having them understand that, though putting forth effort may increase performance, more losses occur due to victim compensation, etc., if an accident is caused. Additionally, they need to understand that it is therefore necessary to take appropriate breaks while driving and to consciously check one's surroundings.

Additionally, as there is a tendency in ITG to–while as a common belief considering the cause of accidents to be one's own lack of effort–describe in the report that the cause of the accident was another party when actually faced with an accident, it is possible that there is a cognitive discrepancy with respect to the common belief and the causal attribution at the time of an accident. When this is not noticed by the persons themselves, the effectiveness of educational efforts aiming for understanding the accident as their own problem will likely also be insufficient. In terms of education, prompting introspection about the cause of the accident one encounters and promoting awareness of the aforementioned discrepancy are thought to be important.

Acknowledgments

This paper is obtained by revision and improvement on the basis of the manuscript of the next conferences proceedings

T. Murohushi, K.T. Nakahira, M. Okamoto, "Study on assessment of participants' theories of intelligence: On the purpose of improvement in safety of car driving." 12th Forum on Information Technology, pp.545-548, 2013

M. Okamoto,"A study on the measure against improvement in safety consciousness of taxi drivers based on safety culture" 28th International Congress of Applied Psychology, Paris France, e-poster, 2014

References

[1]国土交通省大臣官房運輸安全監理官室,"事故・ヒヤリハット情報の収集・活用の進め方～事故の再発防止・予防に向けて," http://www.mlit.go.jp/common/001061869.pdf, April. 2009 (2016.10.3)

[2] N, A. Yamashita, “Study of the Measurement of the Safety Attitude,” IATSS Review, vol.16, no.4, pp.17-24, 1990
[3] Y. Araki, “A review of causal attribution,” Socio-Environmental Studies, vol.5, pp.139-151, Mar. 2000.
[4] C.S Dweck,& E. L. Leggett, A social-cognitive approach to motivation and personality Psychological Review 95, 256-273, 1988.
[5] C.S. Dweck, & A. Master, “Self-theories motivate self regulated learning, “ In: D.H. Schunk & B. J. Zimmerman(Eds.) “Motivation and Self-regulated Learning : Theory, Research and Applications. NJ Lawrence Erlbaum Associates, pp.31-51, 2008.
[6] D.M. VandeWalle, S.P. Brown, W.L. Cron, J.W. Slocum, “The influence of goal orientation and self-regulation tactics on sales performance: A longitudinal field test.” Journal of Applied psychology, no.84, pp.249-259, 1999
[7] Y, Hong, C. Chiu, C.S. Dweck, D.M. Lin, W.Wan, “Implicit theories, Attributions, and coping: A meaning system approach.” Journal of Personality and Social Psychology, no.77, pp.588-599, 1999
[8] M. Nasu, M. Horino, “Causal attributions and achievement-related affects.” Japanese Journal of Educational Psychology, no.39, pp.332-340, 1991
[9] A.G. Greenwald, D.E,McGhee, J.L.K. Schwartz, “Measuring individual differences in implicit cognition : The Implicit Association Test.” Journal of Personality and Social Psychology, no.74, pp.1464-1480, 1998
[10] J.B. Asendorph, R. Banse, D. Mucke, “Duble dissociation between implicit and explicit personality self-concept : The case of shy behaviour.” Journal of Personality and Social Psychology, no.84,380-393
[11] T. Fujii, H. Uebuchi,”Assessment of Participants’ Theories of Intelligence: Reliability and Validity of the Implicit Association Test.” Japanese Journal of Educational Psychology, no.58, pp.263-274, 2010
[12] Greenwald AG, Nosek BA, Banaji MR. Understanding and using the implicit association test : 1. An improved scoring algorism. Journal of Personality and asocial Psychology, no.85, pp. 197-216, 2003.
[13] L. Festinger, “Informal social communication.” Psychological Review, no.57, pp.271-282, 1957

(Received: 7 October 2016, Accepted: 5 December 2016)

Engineering Design Exercise (EDE) for Faculty Development in National Institute of Technology, Nagaoka College

Rumi Shindo Togashi [1,*], Taku Kiryu [2], Shigehiro Toyama [3], Yoshinori Tokoi [4,*], Tetsuro Iyama [5], Fujio Ikeda [6], Yuki Murakami [7], Shin-ichi Akazawa [8], Yasuko Tsuchida [9]

[1)] Division of General Education, National Institute of Technology, Nagaoka College,
[2)] Division of General Education, National Institute of Technology, Nagaoka College,
[3)] Department of Electronic Control Engineering, National Institute of Technology, Nagaoka College,
[4)] Department of Electrical and Electronic Systems Engineering, National Institute of Technology, Nagaoka College,
[5)] Department of Mechanical Engineering, National Institute of Technology, Nagaoka College,
[6)] Department of Mechanical Engineering, National Institute of Technology, Nagaoka College,
[7)] Department of Civil Engineering, National Institute of Technology, Nagaoka College,
[8)] Department of Materials Engineering, National Institute of Technology, Nagaoka College,
[9)] Division of General Education, National Institute of Technology, Nagaoka College,
888 Nishikatakai, Nagaoka, Niigata 940-8532, Japan
**E-mail: rumi@nagaoka-ct.ac.jp*

The National Institute of Technology, Nagaoka College (NITN)'s System Design Innovation Center (SDIC) has launched several systems and tools to encourage research promotion and education reform. Since 2015, SDIC has applied engineering design exercise (EDE) to not only advanced courses students but also new (or "rookie") teachers, the latter of which participate in those courses' advanced experiments as part of their faculty development (FD). This EDE focuses on four competencies: obtaining a fundamental ability for cooperative working, understanding of innovative educational skills, building relationships among teachers from different departments, and creating opportunities for regional contribution. According to a distributed questionnaire to rookie teachers who participated in the class as well as from gathered opinions of managers, we can say that the understanding of active learning and relationship development among new teachers did improve as a result of the EDE. Some participants noted, however, that this program may require much more effort than the organizers expected, so if this EDE is adopted by other institutes, the theme may need to be adjusted to suit the carrier as well as the business volume of participants. We expect that this package can be modified in terms of content to be suitable to each carrier, thereby solving some potential problems.

1. Introduction

National Institute of Technology, Japan (KOSEN) has been required to improve and enhance its education system and to improve the quality of its research. Various measures had previously been taken; for example, the introduction of a model/core curriculum, a quality assurance program to oversee all education at KOSEN, among others. As one of these activities, faculty development (FD) for teachers and staff at the college has been introduced to encourage cooperation and coordination between teachers and staff and to improve individual facilitation and instructional design skills. Each college that is a part of KOSEN conducts lectures or trainings as part of FD, such as instruction seminars at the school, study-abroad programs, and an exchange program between KOSENs. As training for new teachers, some KOSENs have mentoring programs.

The National Institute of Technology, Nagaoka College (NITN)'s System Design Innovation Center (SDIC) has designed several systems and tools to encourage research promotion and educational reform [1]. SDIC has also tried to enhance synergistic effects between active research and education. Since 2013, "advanced experiments" has been required for those students enrolled in advanced courses. During the first semester of the year, engineering design exercise (EDE) was arranged for students to learn how to manage the current rapid technological development and globalization and to cope with recent changes in Japan's industrial structure. EDE is designed to serve as a cross-field education program[2][3]. Within the EDE, instructors use teaching methods such as active learning (AL) and project based learning (PBL).

Since 2015, SDIC has used EDE for not only advanced courses students but also for new (or "rookie") teachers. It expects that the following four competencies will be achieved: (1) learn fundamental competencies for collaborative working, (2) understand advanced examples of teaching methods like AL and recognize essential skills or requirements for advanced knowledge and skills, (3) build relationships among teachers through cooperative research held both inside and outside of the college, and (4) seek opportunities for regional contribution and community involvement. In this paper, we propose and introduce EDE as a training method for rookie teachers. We also share the questionnaire we developed for this group in 2015 and 2016, then discuss efforts, positive outcomes, and problems that may remain to be solved.

Contents of Engineering Design Exercise (EDE) as Faculty Development

EDE is part of advanced courses students' first semester as part of the required subject "advanced experiments." As one part of faculty development and induction, rookie teachers join and participate in this class as students. This experimental attempt started in 2015. In the class, participants practice methods needed for engineering design processes and solve real problems by using these methods. Contents of the current curriculum—the purpose of which is mentioned in Section 1—are shown in Table 1.

Table 1 Contents of Engineering Design Exercise

	Contents	Classes (150 min / ea.)
1. Guidance Logical thinking - Ice-breaker session	A. Need for engineering design exercise (EDE) B. Ice-breaker session	1
2. Logical thinking - Meeting procedures and consensus building	A. Meeting procedures for engineering facilitation B. Workshop (methods for creating new ideas) a. Brainstorming b. KJ method C. Methods for consensus building a. Voting b. Priority decision making matrix c. Identify advantages and disadvantages d. Payoff matrix	1
3. Logical thinking - Idea creation tools and plan proposal	A. Idea creation (how to get to advanced and definite ideas) a. Logic tree (top-down and bottom-up) b. MECE (mutually exclusive and collectively exhaustive) c. TRIZ (Teoriya Resheniya Izobretatelskikh Zadatch) d. Osborn's Checklist B. Plan proposal a. Process to create the plan	1

	b. Requirements for the outstanding plan	
4. Logical thinking - Activities (plan proposal)	Practice methods for the meetings Plan proposal about real problems Preparation for the plan presentation <Examples (real problems)> 1. Development of a management system for compacting concrete 2. Development of river flow velocity measurement techniques 3. Development of teaching materials using LEGO MINDSTORMS® for technical courses in junior high school (theme in 2015 and 2016 for rookie teachers)	2
5. Engineering facilitation - Presentation of planning	Plan presentation and exchange of opinions among students in the class, teachers and staff in the school, teachers in the junior high school, and supporting companies Objective: Improvement of plan	1
6. Engineering facilitation and planning for design theme - Activities (improvement of plan)	Trial-based PDCA cycle (e.g., "plan, do, check, act") Improve the plan, based on opinions, comments, and potential problems obtained at the plan presentation Practical use PDCA cycle	3
7. Planning for design theme - Design review	Simple presentation and exchange of opinions between groups dealing with the same theme Decision on the final plan	1
8. Planning for design theme - Preparation for presentation of outcomes	Trial-based PDCA cycle Prepare device, system, documents, etc. for result presentation	4
9. Presentation of outcomes	Results presentation for students in the class, teachers and staff in the school, teachers in the junior high school, and supporting companies Evaluate the plan	1

Investigation of the Effect of EDE as FD

This study used a questionnaire survey at the end of the in-class EDE in 2015 and 2016. The questionnaire consisted of 13 questions that asked trainees about their feelings and perceived difficulties throughout the EDE (Table 2).

Table 2 Questionnaire items

Q1. What was the proportion of work for EDE compared with your overall workflow?
Q2. Did you get a sense of the temperament of the Nagaoka KOSEN (NITN) students (i.e., advanced courses students) in EDE?
Q3. Do you think EDE should become one option for teachers' faculty development?
Q4. The attempt to train new teachers along with students in EDE started in 2015. Do you think it is a good idea to continue this next year?
Q5. Have the relationships among new teachers deepened through participation in EDE?

Q6. What do you think about the difficulty of this year's design theme to develop technology materials for a junior high school?
Q7. Did you have enough time in the class to carry out the design theme?
Q8. Did you need extra time to work on the design theme outside of your regular EDE class?
Q9. Please tell me some good points and not-so-good points of EDE as FD.
Q10. In EDE class, the ways of logical thinking and engineering facilitation, such as meeting procedures, consensus building, and plan proposal are presented. Have you previously participated in a class or training session related to such facilitation skills?
Q11. In EDE class, what theme(s) do you see as being utilized in the future? (You can provide multiple themes.)
Q12. Were you able to deepen your understanding of AL due to participation in the EDE class?
Q13. EDE is supported by local companies, elementary schools, and junior high schools. EDE education can provide measurable opportunities to contribute to the local community. Was there any change in your opinion about the importance of this education to contributing to the local community?
Q14. Please freely express your opinion or impression of EDE (e.g., did you notice possible improvements to the theme that could be made next year?).

Questionnaire Survey Results and Discussion

The significant results of the questionnaire are shown in Figs 1 through 8. Fig. 1 reveals that all trainees, both in 2015 and 2016, recognized the effect of EDE as FD, and in Fig. 2, trainees answered that it was possible to interpret the students' temperament. On the other hand, results in Figs 3 through 8, which are concerned with the EDE program itself, are different when comparing the years 2015 and 2016. The design theme in EDE class was the same in 2015 and 2016, so this discrepancy probably came from the difference in the required effort of the majority of trainees. Fig. 7 shows that the effort needed for EDE varied among trainees and Fig. 9 shows that most trainees were able to learn more about the AL method.

Moreover, the responses to Q9 ("Please tell me some good points and not-so-good points of EDE as FD") included the following. As the good points: "We can work with teachers who have different professions," "lectures on the conference method and consensus making were taught before tackling the problems," "we came to have further interest in students' research and activities, knowing first-hand what the students learn." As for the not-so-good points: "It was absolutely impossible to finish the activities for EDE within school hours."

In addition, responses to the open-ended Q14 ("Please freely express your opinion or impression of EDE"), one opinion was as follows: "It should be discussed whether the participation of rookie teachers should be voluntary or mandatory."

From the above, it is clear that participants were able to understand the temperaments of the students and understand the effects of AL as FD through the lectures about meeting method and consensus making. While trainees considered that collaborating with teachers from different fields was a key advantage, it was revealed that there was a difference between the trainees' required effort. In addition, only one of the trainees reported that the relationship among trainees worsened as the EDE progressed. This may be due to the difference in trainees' awareness regarding the importance of their participation in EDE. Solving this problem will require further improvements to activity efficiency.

As the background instruction of this EDE as FD is carried out, training or induction into a class

that already exists could reduce or, in some cases, eliminate the cost to invite more instructors. Attending the lectures for students, however, in addition to their usual work may feel like excessive effort to some trainees. Also, newly appointed teachers who are considered “general educators” may lack even a base level of engineering knowledge, which may result in more time required to understand the contents of EDE.

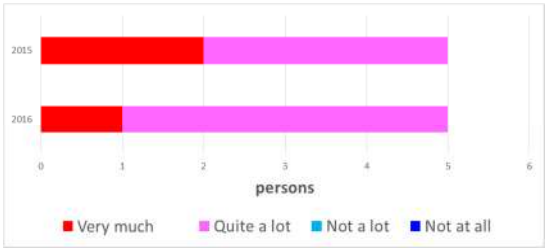

Fig. 1 Survey result (Q3)

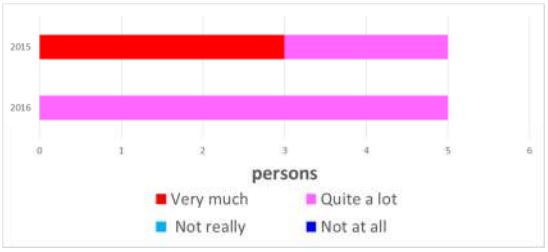

Fig. 2 Survey result (Q2)

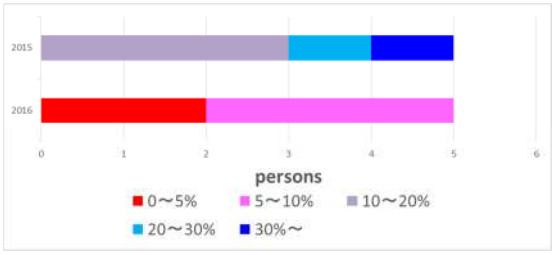

Fig. 3 Survey result (Q1)

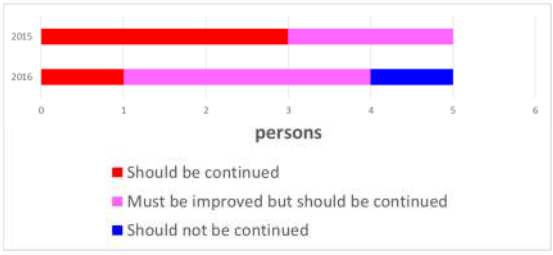

Fig. 4 Survey result (Q4)

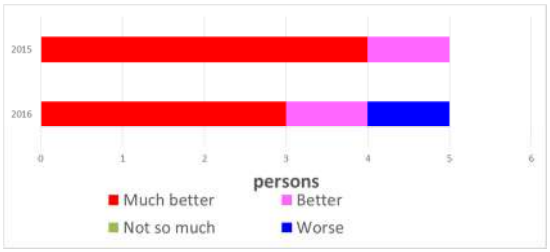

Fig. 5 Survey result (Q5)

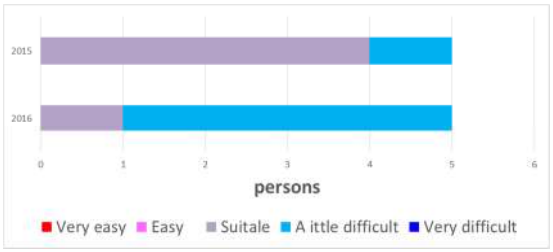

Fig. 6 Survey result (Q6)

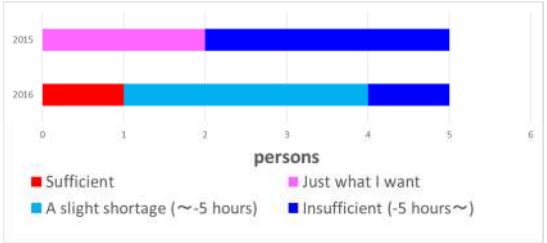

Fig. 7 Survey result (Q7)

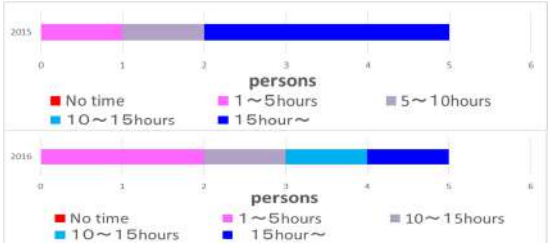

Fig. 8 Survey result (Q8)

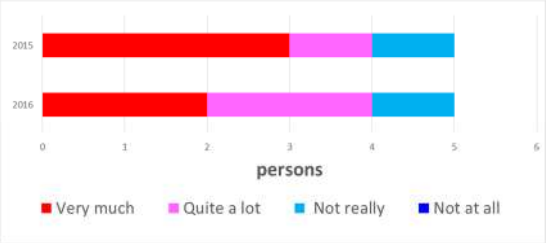

Fig. 9 Survey result (Q12)

Conclusion

EDE utilizes the required subject of advanced experiments as an FD opportunity for rookie teachers. This attempt started in 2015 and aims to build fundamental competencies for collaborative working, understanding and obtaining the skills required for those in higher education, building relationships among teachers across different departments, and creating opportunities for regional contribution. In an EDE class, logical thinking and engineering facilitation, such as meeting procedures, consensus building, and plan proposal are presented. EDE participants try to solve real problems using their skills and materials and methods presented in the lectures and then present the outcomes. According to the results of the questionnaire provided to the participant rookie teachers, it is clear that their understanding of active learning and the relationships among the new teachers became better, while some considered that this program required much more effort than initially expected. As such, if this EDE is adopted by other institutes, the theme should be customized to suit the carrier as well as the business volume of participants. We expect that this package and system can be improved and result in positive effects by modifying or customizing the content to be more suitable to each carrier, solving their unique potential problems.

Acknowledgments

The authors wish to express gratitude to the supporting companies, participants and co-operators of the education component, rookie teachers who joined the class, colleagues in SDIC, and NITN, the latter of which were crucial to permitting these trials in the first place.

References

[1] Toyama, S., Ikeda, F., Iyama, T., Tokoi, Y., Akazawa, S., Murakami, Y. and Tsuchida, Y., System Design Education Program to Produce Innovative Personnel, Transactions of ISATE 2015, (2015) 277-280.
[2] Iyama, T., Toyama, S., and Tokoi, Y., A Practice of Engineering Design Education through the Development of Educational Materials using LEGO-Mindstorms, The 4th International GIGAKU Conference in Nagaoka, EO-17, (2015).
[3] Toyama, S., Miyakoshi, K., and Tasaki, Y., Design and Practice of Engineering Design Education, *Journal of Education in Japanese College of Technology*, No.38, (2015) 67-72.
[4] Maeno, T., *Official Guide Book to KEIO SDM: System and Design Thinking for Creating Innovation.* Tokyo: Nikkei BP, (2014).
[5] Oishi, K., *Engineering Facilitation*. Tokyo: Morikita shuppan, (2011).
[6] Pink, D.H., *High Concept, the times of innovative personnel*, translated by Kenichi, O., Tokyo: Mikasa shobo, (2006).

(Received: 6 October 2016, Accepted: 6 December 2016)